8-2015

Two dimensional inverse dynamics model of human knee dynamics during the moderate squat exercise

Ricardo Gomez Jr.
University of Texas-Pan American

TWO DIMENSIONAL INVERSE DYNAMICS MODEL OF HUMAN KNEE DYNAMICS DURING THE MODERATE SQUAT EXERCISE

A Thesis

by

RICARDO GOMEZ JR.

Submitted to the Graduate School of
The University of Texas-Pan American
In partial fulfillment of the requirements for the degree of

MASTER OF SCIENCE

August 2015

Major Subject: Mechanical Engineering

TWO DIMENSIONAL INVERSE DYNAMICS MODEL OF HUMAN KNEE DYNAMICS DURING THE MODERATE SQUAT EXERCISE

A Thesis
by
RICARDO GOMEZ JR.

COMMITTEE MEMBERS

Dr. Dumitru Caruntu
Chair of Committee

Dr. Javier Kypuros
Committee Member

Dr. Mataz Alcoutlabi
Committee Member

August 2015

ABSTRACT

Gomez, Ricardo, Two Dimensional Inverse Dynamics Model of Human Knee Dynamics during the Moderate Squat Exercise. Master of Science (MS), August 2015, 78pp., 32 figures, references, 45 titles.

The purpose of this research is to investigate the internal forces on the human knee joint during moderate squat exercise. An inverse dynamics, two dimensional, anatomic dynamic knee model is developed. The model describes the motion in the sagittal plane of human leg, and includes tibia, femur, ligamentous knee structures, tendons and muscles. The software package Matlab is used to solve the inverse dynamics model. Numerical simulations are conducted for walking (the stance phase of the gait cycle) in order to validate the model, and for moderate squatting in order to predict ligament, contact and muscle forces during this exercise.

DEDICATION

The accomplishment of my graduate studies is due to the numerous sacrifices, and unmeasurable support of my family. Thank you for believing in me and for all your love that inspired me to achieve this degree. I have a special feeling of gratitude to my loving parents, Ricardo and Rosalinda Gomez whose words of encourage helped push me throughout my research.

I also dedicate this thesis to my many friends who have supported me throughout the process. I will always appreciate them for sharing their memories and experiences with me and enlightening me over the many years of friendship.

Last, but certainly not least, I dedicate this thesis to Vanessa Gonzalez, for her motivation and making a real difference in my life. I will always treasure our relationship and think of you with warm feelings, and a special place in my heart.

ACKNOWLEDGEMENTS

This work has been accomplished at the Department of Mechanical Engineering at The University of Texas – Pan American. I would like to thank the University for allowing me to use the research facilities.

I wish to thank Dr. Dumitru Caruntu for allowing me to pursue my thesis under his supervision. He provided ample amounts of guidance in this thesis and extreme helpfulness in directing me on how to approach and conduct this research, who helped whenever I was in need. He helped me with my questions and doubts.

I would also like to thank the committee members Dr. Kypuros and Dr. Alcoutlabi for their comments and suggestions regarding my thesis. I also appreciate all the knowledge and wisdom passed on to me over the years by the Mechanical Engineering professors at The University of Texas – Pan American.

TABLE OF CONTENTS

Page

LIST OF FIGURES

Page

CHAPTER I

INTRODUCTION

Understanding of the anatomy of the knee joint is essential to the formulation of any type of model. Since the development of input information for a model is not easily attained, this section will discuss the basic anatomy of the knee joint, and the different techniques used to obtain the anatomical information used to produce a model, and why a better understanding of why the joint is important.

The knee is the most investigated joint in the human body. It is the most heavily loaded and mobile joint with the highest incidence of osteoarthritis and injuries.

The knee joint contains three bones that allow motion to occur; the femur (thigh bone), tibia (shin bone), and patella (knee cap) shown in Fig. 1.1. Friction between their surfaces, can be neglected due to the fact that each bone is covered in a smooth yet hard material known as articular cartilage, (Goldblatt and Richmond, 2003).

The femur and tibia bones are connected by a number of ligaments which account for the majority of the stability of the knee. The Anterior Cruciate Ligament (ACL) runs from the anterior (front) of the tibia to the posterior (back) of the femur (Abdel-Rahman and Hefzy, 1993; Mosouros et al., 2010). This ligament helps in the prevention of forward motion of the tibia, and is known as the most commonly injured ligament.

The Posterior Cruciate Ligament (PCL) runs from the posterior of the tibia to the anterior of the femur and is wrapped around the ACL where they meet between the two bones (Goldblatt

and Richmond, 2003). The Lateral Collateral Ligament is found on the lateral (outer) side of the femur and connects it to the fibula, it also protects the knee joint from various (inner) forces (Sugita and Amis, 2001). The Medial Collateral Ligament (MCL) is located on the inner surface of the femur and connects it to the inner tibia, this ligament resists valgus (outer) forces (Gardiner et al., 2001).

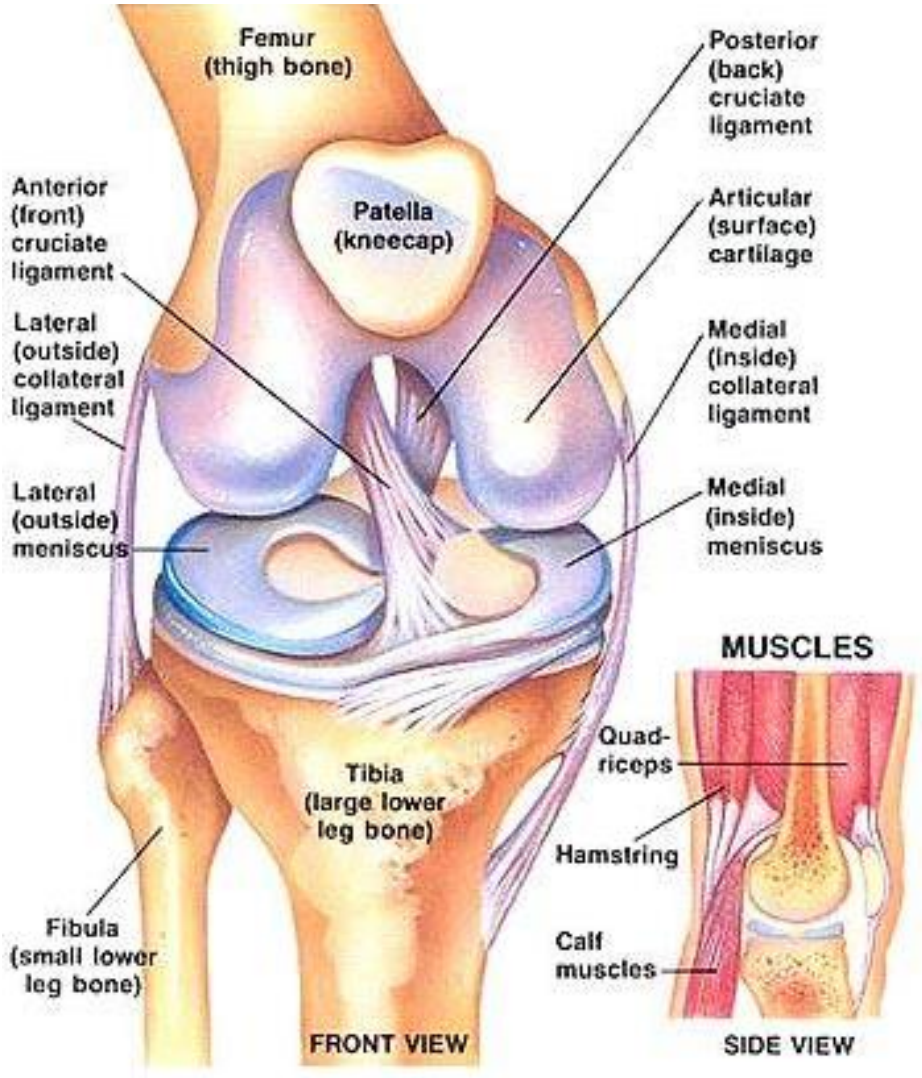

Figure 1.1 View of anatomy of human knee.

http://hipandkneeclinics.com

Based on an anatomically based knee model, to include the ACL, LCL, MCL, PCL, and meniscus (Pena, 2006) found that the ligaments support different loads throughout the range of the knee extension and the menisci spread the axial loads along the tibial plateau.

Two main co-contractor muscle groups that are of concern to the knee are the quadriceps and hamstrings muscles. The quadriceps is the knee extensor muscle and it is comprised of four individual muscles; rectus femoris, vastus lateralis, vastus medialis, and vastus inermedius. The quadriceps muscle is connected to patella through the quadriceps tendon. The hamstrings is the knee flexor muscle. Co-contractor muscles besides actuation maintain the stability of the joint.

Fluoroscopy has been used to obtain information on the motion and geometry of the knee joint. Fluoroscopy is an imaging technique used to obtain real time images; the fluoroscope has an *x-ray* source and fluorescent screed, the patient is placed between these two components of the machine and it produces images of the patients' internal structures (Li and Vandeveldi, 2008). Another technique for developing a geometric model on the insertion points of a knee is using Magnetic Resonance Imaging (MRI) technology (Li et al., 2001).

In vivo studies using the fluoroscopic imaging technique are being used to both validate and improve existing models. Two particular knee models were found in which the fluoroscopic imaging was used to generate a model for analysis. In both cases the accuracy of the images was described as either accurate or relatively accurate (Shelburne and Pandy, 1996). From the imaging techniques more accurate geometric measurements are made, which will allow for better results from the models.

One technique for developing information on the kinematics of the knee joint involves reflective markers, which act as nodes that are attached to the skin and in some cases directly to the bone. The nodes are monitored by multiple, strategically placed, video cameras that can

generate a three-dimensional kinematic data for the joint. The reflective markers that are attached to the bone are used to eliminate any error in motion due to the motion of the skin over the knee joint.

An anatomical dynamic model including the femur, tibia and patella was developed in order to determine a three-dimensional dynamic response of the knee (Caruntu and Hefzy, 2004). Throughout the entire range of motion, the medial component of the tibio-femoral contact force was found to be larger than the larger than the lateral force, while the lateral component of the patella-femoral contact force was found to be larger than the medial one and the ACL and PCL had opposite force patterns.

The purpose of this research is to investigate the forces on the knee joint during a deep squatting exercise. An anatomic 2D dynamic knee model is used in the sagittal plane and includes force contact, ligaments, forces on the ligaments, tendons and muscles and is fully dynamic. Two movements investigated are gait cycle and moderate squat exercise. The system of dynamic equations is used as equality constraints in a nonlinear programming algorithm that minimizes the forces in the system. Matlab function fmincon is used to solve the nonlinear optimization of the model.

2.1. Justification for the Research

Obesity has been increasing in the United States and the rest of the world and this causes many health concerns including musculoskeletal disorders of the knee joint due to the extra load and forces on the knee joints. The leading cause of a knee replacement is osteoarthritis and is the principal diagnosis of 96% of TKR recipients. Approximately 12% of adults over 60 have symptoms of knee osteoarthritis. In 1990, 21 million Americans had osteoarthritis, with that number increasing to 27 million in 2009, and in the year 2030, over 67 million American are

expected to suffer from osteoarthritis. Osteoarthritis was the 4th most frequent principal diagnosis for hospital stays in 2009. Knee osteoarthritis and general knee pain, are the leading causes for disability amongst the elderly, and are increased when those are obese. In 2009, knee replacement was the 14th most common inpatient procedure. More than 4.5 million Americans are currently living with at least one Total Knee Replacement (TKR), and make up 4.7% of the population age 50 years or older. Over 650,000 knee replacements occurred in 2010. Less than 10% of knee replacements are partial knee replacements and all others are total knee replacements. 5% of patients have both knees replaced at the same time. Over the age of 50 5.3% of American women and 4.1% of men have at least one TKR, (Weinstein et al., 2012). Three-dimensional finite element (FE) models can help provide a method to systematically evaluate the consequence of biomechanical risk factors on the knee joint, without the additional influence of confounding factors, by analyzing the stress and strain throughout the lower body. This study will use lower body motion analysis and forces plates as a tool to investigate the effect of obesity and distribution of forces onto the knee, by predicting the stress and strain forces the knee is experienced during squatting. The squat exercise is becoming increasingly popular in clinical settings as a means to strengthen lower body muscles and connective tissue after joint related injury. The squat exercise has been used for treatment of ligament injuries, TKR, and ankle instability. Also, there are less forces acting upon the anterior cruciate ligament (ACL) than the knee extension making squats a better rehabilitation exercise for an ACL injury.

The squat exercise is one of the most common daily activities, and it involves almost every muscle from the waist down. The gluteus group and deep hip muscles, quadriceps and hamstrings are very important in this exercise. Other muscle groups, such as the abdominals, spinal musculature, and calves are also used to stabilize the body and keep you from falling over.

In the gym, squatting is one of the best exercises to train lower body, but it is also one of the most challenging and controversial. Squatting is used in many sports routines designed to enhance athletic performance. However, squat performance are not limited to the athletic population. Given that most activates of daily living use the coordinated interaction of numerous muscle groups in a single maneuver. The squat exercise has a close specificity to many everyday tasks such as lifting packages, picking up children and many others.

Considering the complexity of the exercise and the many variables related to performance, understanding squat exercise biomechanics is of great importance for achieving optimal muscular development, reducing the chance of a training related injury, as well as how obesity will effect forces on the knee. Understanding the effect of the kinematics and kinetics of the squat exercise on the joints and muscles forces is important in order to provide recommendations, optimize the performance of squat exercise and reduce osteoarthritis in patients for a healthy and pain free lifestyle.

CHAPTER II

REVIEW OF LITERATURE

Models can be classified into two types: anatomically based models, and phenomenological models. Phenomenological models are general models that take the part as a hole, so the analysis is done on the entire body and the interest is in the overall response of the object. Anatomically based models look at individual components of the structure, so the accuracy of the model is of importance. Anatomically based models can be divided into two sub-groups: kinematic and kinetic models. Kinetic models use the loading constraints to relate the parameters of motion, whereas kinematic models don't need the loading conditions to relate the parameters.

In previous investigations two-dimensional representations of the knee joint were used. There models were useful when it came to predicting joint kinematics in the sagittal plane. However for internal-external rotations or medial and lateral tibio-femoral contact forces three-dimensional models are needed. (Blankevoort and Huiskes, 1996) created a 3D mathematical model of the tibio-femoral joint whose motion was dependent on equilibrium forces and moments. (Bendjaballah et al., 1995) investigated the overall response of the knee using a Finite Element model and later (Peña and Calvo, 2005) presented a 3D FE model that analyzed the behavior of ligaments and the role they play in knee stability. (Abdel-Rahman and Hefzy, 1997) reported the dynamic response of a 3D model that used DAE's (differential-algebraic equations) to solve the system of equations of motion.

2.1. Anatomy

The knee joint is a unique joint in the human body. The knee joint kinematics is not similar to a hinge, i.e with a set axis of rotation, but rather bends along a constantly changing axis. The knee is made up of three bones femur, tibia, and patella. The amount of friction between their surfaces is very small due to the articular cartilage covering each bone and the synovial fluid of the joint itself. These bones are connected by a number of ligaments which account for the majority of the stability of the knee as shown in Fig. 1.1. The knee flexor-extensor muscles are hamstrings, quadriceps, and gastrocnemius.

2.2. Injuries, Diseases, and Treatments

Knee joint osteoarthritis, ligament ruptures, implant failure, and wear of articular cartilage are some of the causes of injuries in the knee joint. The environment the knee is subject to is crucial for proper prosthetics design (Perez-Gonzalez et al., 2008), as well as for prevention of the degeneration of the knee joint, (Bei, 2004). This section will focus on the known injuries, treatments that are common in the knee joint, and related studies.

2.2.1. Injuries.

Minor knee injuries such as knee paint, joint swelling and knee instability, are seen with frequency in the emergency room. Minor knee pain is usually caused by arthritis, a fluid filled swelling, and inflammation due to over use or torn meniscus. Joint swelling is the buildup of fluid in the soft tissue surrounding the bycondular knee joint. This can be caused by arthritis, lupus, or hemarthrosis, (Savio et al., 2006). The stability of the knee is partially given by the ligaments. There exist three levels of severity for ligament injuries:

- Grade I: Some tenderness and minor pain at the point of injury. This means there has been small tears in the ligament.

- Grade II: Noticeable looseness in the knee (knee opens up about five millimeters) when moved by hand. There is major pain and tenderness on the inner side of the knee as well as swelling. This means there are larger tears in the ligament, but it is not torn completely.
- Grade III: Considerable pain and tenderness at the inner side of the knee; some swelling and marked joint instability. Knee opens up slightly less than half an inch when moved. A grade III LCL tear means that the ligament is completely torn. There may also be a tear in anterior cruciate ligament.

The fracture of bones also affects injuries seen in knees, when a bone if fractured the forces due to loading are redistributed and may injure other components the system.

2.2.2. Diseases

Osteoarthritis can be defined as the degradation of articular cartilage. This occurs when the combination of mechanical wear and biochemical degradation erodes the cartilage, which this leads to bone to bone contact, which can be very painful.

2.2.3. Treatments

Non-surgical treatment is used for grade I and II injures. Treatment includes applying ice to the injured area, raising the knee above heart level, and non-steroidal anti-inflammatory drugs (NSAIDS). One should limit physical activity until the pain and swelling go away, braces and casts are usually used to limit the range of motion in the knee for the surrounding ligaments. Once the swelling has subsided physical therapy is usually recommended to build strength in surrounding muscles that will re-stabilize the joint.

Most rehabilitation plans include:

- Passive range-of –motion exercises designed to restore flexibility
- Braces to control joint movement
- Exercises to strengthen the quadriceps muscles in the front of the thigh. Muscle strength is needed to provide the knee joint with as much support and stability as possible when weight is placed on it.
- Additional exercises on a high-seat exercise bicycle, followed by more strenuous quadriceps exercises.

Surgical treatments in ligaments are more common. Since 1991 doctors have used the allograft method to reconstruct grade II injuries of ligaments, Fig. 2.1. Surgeons take graft tissue from a tissue bank and replace the damaged ligament. The allograft is bone tendon that is fasted with interference screws to both the fibular head and femur.

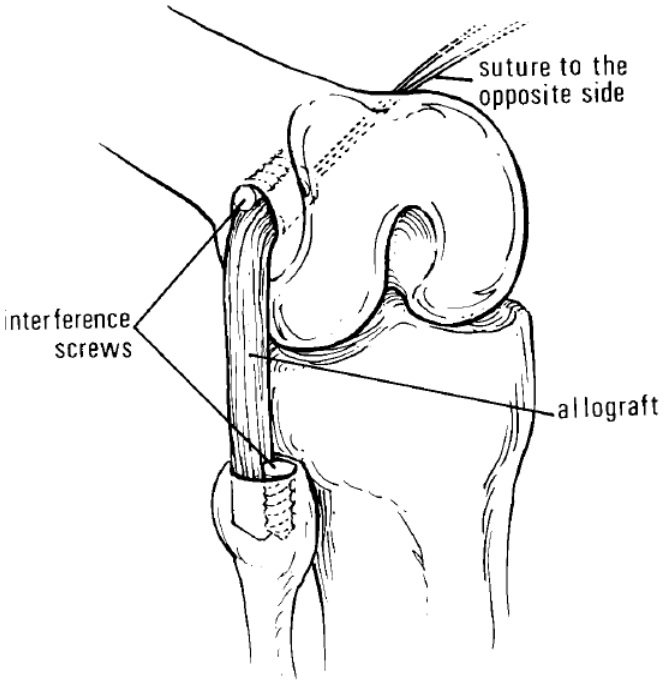

Figure 2.2 View of allograft.

The autograft method is exactly like the allograft method with one difference. In this procedure tendon from your own body, usually your hamstring is removed and grafted to the correct dimensions then fastened to the bones with staples. During the procedure of ligament tightening the surgeon takes the remaining ligament and detaches one side from the bone, then proceeds to reduce the length of the ligament and rejoins the band to its corresponding bone with a series of staples. Ligament repair is performed when a recently operated ligament is pulled from it attachment. A small incision is made just above the site and stitches or structure anchors (special staples) are used to reattach the ligament to the bone.

Post stiffness in ligaments that have undergone reconstruction has been reported, and a loss of motion from 4% to 38%. In reference, (Robertson, 2009), suggests that with this comes a risk of multiple-ligament injuries, poor range of motion in the joint and poor compliance with rehabilitation. Successful recovery is defined as a loss of extension of less than 5˚, and flexion less than 15˚ within 3 months.

In reference, (Robertson, 2009), investigated 100 patients that underwent ACL reconstruction with quadruple hamstring autografts. The average age of the patients was 30 years. On average a delay of 15 months was set between the injury and the surgery to allow for proper pre-operative conditions to be met. An arthroscopy of the knees was done in order to identify tears and lesions in the ligament. After the surgery, an assessment of the range of motion was made for each patient. Required rehabilitation was prescribed to the patients. In 6 weeks 66% of the patients had a successful recover, after 6 months 88% of patients had fully recovered, and 95% reported success after 12 months.

Knee replacements have been used since the 1970's. For patients with osteoarthritis since the surface of the joint has seen enough degradation to be labeled as "worn out," a total knee

replacement, i.e. resurfacing of the knee, is necessary. In this case the bones are covered with metal and plastic to create a smooth motion. Success rates in knee replacements are approximately 90%. Some complications have been seen as a result of infections of the prosthesis, if this occurs antibiotics are administered and the re-implantation in attempted. After the implantation is complete it takes anywhere from three week to two months for a full recovery. Daily activities are no problem, but it has been mentioned that prosthesis is not designed for impact loading activities.

2.3. Experimental Work

(Li and Vandeveldi, 2008) conducted an in-vitro study of two cadaveric knees. To obtain the geometry of the structures magnetic resonance images (MRI) were used, it was mentioned that a the fluoroscopic mages of dynamic motion along with the geometric information from the MRI scans produced enough information to determine the 6DOF dynamic kinematics of the knee. In this study three ceramic beads were imbedded in the tibia and femur of the two cadaveric knees. MRI scans were taken of the knees using a 3.0T magnet, the images were used to construct a 3D model of the bony structures and the positions of the ceramic beads. The knees were then separately placed between two fluoroscopic screens and the images of two separate views were recorded at a rate of 30 frames per second while the knee was in motion, thus producing the path of motion for a cadaveric knee.

In vivo studies using the fluoroscopic imaging technique are being used to both validate and improve existing models. Two particular knee models were found in which the fluoroscope was used to generate a model for analysis, in both cases the accuracy of the images was described as either accurate or relatively accurate. In reference, (DeFrate, 2004) studied the contact between tibial and femoral cartilage during knee flexion. Five human subjects (21-

41years old) with no previous history of knee injuries were used for this study. Magnetic resonance images were taken of each subject; the images were then manually traced in a solid modeling software and used to generate a 3D model. Each subject was performed lunges in for distinct positions between two fluoroscopic imaging screens; the images were imported into the solid modeling software. A previous study confirmed that the model was accurate within 0.1mm in translation and 0.1˚ in rotation (Li and Vandeveldi, 2008).

(Shelburne and Pandy, 1996) used a two-dimensional model to analyze the limits of the human knee joint. Twenty three cadaveric knees were used to determine the two dimensional curves of the lateral femoral condyles and the femoral groove. The tibial plateau was simplified to a flat surface with a slope of 8˚, the patella was assumed to be rectangular, and all surfaces were assumed to be frictionless. Three coordinates were used to describe the placement of the bodies. Anterior-posterior translation (front and back), proximal- distal, which describes the closeness to the midline of the body, and the angle between the axis of symmetry of the femur and tibia. Using the software package SD/Fast the equilibrium equations along with the constraints of the system were obtained. The ligaments were modeled as straight lines that were assumed to be elastic and the mechanical properties were taken from patterns that resulted from previous studies such as (Blankevoort and Husiskes, 1991). The muscles were modeled in a similar fashion. Three positions were tested: quadriceps leg raise, maximum extension, and flexion. A system of equations was generated with the unknowns, so using a nonlinear programming algorithm the system of equations was solved.

Another issue with the knee joint is accurate diagnosis and treatments of injuries. Further research was needed to determine ligament and tendons insertion locations. During surgery the attachment sites of interest can be difficult to find. (LaPrade, 2000) used cadaveric knees of 10

frozen specimens, which had no prior surgeries or abnormalities to study the anatomic attachment sites of ligaments and tendons. The average age of the specimens was 63, which is reasonable since the majority of the patients with chronic knee injuries are older people. The specimens were dissected and the skin, muscle, and soft tissue were removed from the tibia and the fibula, so that the specimen could then be mounted onto the testing machine for analysis. Each knee was potted and screwed into place to prevent any rotation during the analysis. Once the specimen was secure additional dissection was performed to identify the components of interest and their insertion sites.

Another investigation using 10 frozen cadaveric knees was used to determine the average geometry and mechanical properties of the components of the knee joint (Sugita and Amis, 2001). The average age of the specimens was 70 years. The previously dissected knee joints were potted in a stainless steel cylindrical tube using polymethyl methacrylate bone cement. Screws were used to fix the tibia and fibula firmly in place. Attachment sites of interest were identified and marked with pins; a camera was set up on a tripod and recorded the position of each pin. The positions of the pins were recorded for knee flexions of 0˚, 30˚, 60˚, 90˚, and 120˚. The specimens were then prepared for tensile testing. Using an Instron 1122 materials testing machine each specimen was mounted and extended to failure at 200 mm/min. The strains were calculated from the generated information. This type of study (quantitative and qualitative studies) has been proven to be extremely essential to the clinical experiments that use any kind of software, for the purpose of validation of generated data. It was made clear that a precise understanding of the biomechanics of structure is vital to clinical attempts at repair and any kind of design analysis such as constraint equations used in software programs, (Masouros et al., 2010).

Accurate measures of the level of injury when it comes to ligaments are still under investigation. An attempt to determine the effectiveness of certain methods tested magnetic resonance imaging (MRI). Thirty MRI scans from diagnosed subject with normal, partially torn, and completely torn ligaments were taken closely analyzed. The patients were diagnosed using arthroscopic surgery, in which a small camera is inserted into the joint and other instruments are inserted through small incisions to repair the ligaments. Upon careful review of the MRI scans 100% of the fully torn ligaments were correctly diagnosed, 92% of ligaments in normal conditions were correctly diagnosed, but only 11% of partially torn ligaments were diagnosed correctly. The MRI scans proved to be a fairly accurate form of diagnosis, for anything but partially torn ligaments, in order to compensate for the failure of the MRI scans ultrasound testing was conducted. This study proved that ultrasound testing of injured sites is an effective alternative to MRI scans for the evaluation of soft tissue, and diagnosis of several other abnormalities.

In reference, (Shelburne and Pandy et al., 1996) used the software package SD/Fast to model the knee for evaluating ligament forces. They used eleven separate bundles for modeling ligaments, assumed to be elastic, and capsular structures. Values used to create the model (mechanical properties, and geometry) were based on previously published journals under the same conditions and loads. Once the model was complete it was used to analyze forces produced in the ligaments under maximum condition. (Shelburne and Pandy et al., 1996) generated static equilibrium equations, containing vectors of gravitational forces, torques, moment arms of contact, and ligament forces. They reported that the model was able to reproduce many of the characteristics (patterns) of a three-dimensional knee under the same conditions.

In reference, (Peña et al., 2005) compiled a complete 3D finite element model of the human knee that includes all joining ligaments, menisci and articular cartilages that included initial forces and stresses, to simulate as real a model as possible. In the past it has been seemingly impossible to simulate an accurate account of a natural situation, because the musculoskeletal system is so complex and the constitutive equations describing the behavior of joints are far from ideal. (Peña et al., 2005) used nuclear magnetic resonance (MRI) for soft tissue, and computed tomography scans for bones to obtain the geometrical data needed for the model. With the help of the medical doctors from the Traumatology Department of the University of Zaragoza they identified the locations of areas of interest. They used a total of 5195 eight- node brick elements for the meshes of cartilages, menisci and ligaments. With the software used by (Pena et al., 2005) a finite element model of the anterior and posterior view of the knee joint was generate using a total of 4783 four node surface elements to mesh the bony surfaces, and 195 eight node brick elements to mesh the cartilages, menisci, and ligaments. They used tri-linear hexahedral elements with a nonlinear formulation. The mesh was validated by comparing it to an idealized model; the mesh was found to be within a 4% theoretical error. Each node was custom designed with constraints such as degrees of freedom and placement (usually at center of gravity or center of rotation). The ABAQUS v 6.2 was then implemented with the constitutive model to yield a numerical model that was validated with analytical solutions from previously published journal, (Kanekasu et al., 2004). When modeling the ligaments they made two assumptions. First that there existed no difference in the material behavior, and second that the material characteristics that depend on time (viscoelasticity, creep and relaxation) were neglected. The accuracy of these models depends highly on the geometrical construction and

mathematical constraints describing the behavior of the tissue relevant to motion and interactions with its surroundings, (Mommersteeg and Blankevoort, 1996).

2.4 Soft Tissue Modeling

In reference, (Peña, 2005) used mathematical expressions to simulation the behavior of soft biological tissues in the finite element model created. The behavior of the material was the primary concern, because the ligaments act as bands, which are not completely rigid or entirely elastic. The Cauchy-Green strain measure was used to constrain the deformation of the ligaments. It is well known that with age and cyclic loading the functionality of the joints and their accompanying components begin a degenerative process, for this reason (Peña, 2005) described the volumetric and isochoric responses to the material. They used the free-energy function, where constants are given, and generalized the equation so that it could better satisfy the material constraints, seeing that they assumed that collagen fibers in ligaments do not support compressive loads. (Peña, 2005) included initial strains to better simulate the knee in its actual environment they modeled all ligaments as hyper elastic and transversely isotropic, which includes the effect of a family of fibers, which is often applied to ligaments.

2.5. Modeling and Software Packages for Simulations

Modeling is used for design, analysis and control purposes. Analysis is performed to determine the response of a system under given conditions. Using this analysis, the design of the system can be improved, and finally control systems can be implemented to achieve the desired states.

Knee joint models are complex and the assistance of a computer is almost always needed. Computational analysis allows for optimization of the system. This section will briefly introduce

computer models that have been produced in the past and the software that have been used to generate them.

In reference, (Shelburne and Pandy et al., 1996) developed a two-dimensional model of the knee using equations that were obtained by the software package SD/Fast (Symbolic Dynamics, 1992). Developed by Michael Sherman and Dan Rosenthal of Symbolic Dynamics Inc. SD/Fast provides physically based simulations of the mechanical systems by taking descriptions of the system of rigid bodies, or bodies connected by joints, and derives full nonlinear equations of motion. This software is used to perform analysis and design studies on any mechanical system which can be modeled as a set of rigid bodies connected by joints, and subjected to forces. The system of equations generated are governed by constrain equations. Even though the model constrains the motion to the sagittal plane, because it is a 2-D model, it was concluded that the model closely compares to experimental data. These types of models predicted the response of the system, such as motions and forces, but calculating stresses and strains of the system was a challenge, so the finite element (FE) model needed to be used.

Finite element model have been generated with the commercial code IDEA v9.0 where the main surfaces and solid version of the model were reconstructed with an accuracy of 0.5mm (Pena, 2005). Similar in functionality is Femap Version 9.1 created by UGS Corp., a leading global provider of software and services of pre- and post-processing finite element modeling applications. Femap v. 9.1 is a user friendly program that can easily be used occasionally and by experts, while sustaining a high level of accuracy. This program, in association with Solid Edge V18 (leading software in the production of geometry), has effectively created powerful customization tools to enhance geometry transfer for a more accurate analysis. ABAQUS is a finite element package to develop a dynamic model and perform a finite element analysis. It can

be used to recreate the geometry of the part or assembly, and define each part's material properties and boundary conditions.

In the past, investigations were unable to develop exact mechanical properties and behaviors in the human knee because of certain limitations that hindered experimental studies, such as inaccurate measurements, high costs, and the reproduction of certain situations. A major goal of clinical experimentation is the recreation of a normal joint loading environment under typical loads (Chow et al., 2006). Finite element analysis (FEA) now offers new insight into mechanical behaviors of biological tissues, and has significantly eased excessive cost and time that were once spent for these studies. Finite element models are used to predict the effect of loads, forces and other variable parameters that would be difficult or even impossible with clinical experimentation, (Halloran and Petrella, 2005).

In reference, (Pena, 2006) investigated the knee extension exercise using an anatomically based model, with the ACL, LCL, MCL, PCL, and meniscus to better understand the combined behavior of each component. It was found that the ACL supported 75% of the total anterior load, and was relaxed, or had no part in the resistance of the posterior load. The MCL supported 25% of the anterior load and was relaxed during the posterior load, and was the primary component in the restraint against rotary loads. The PCL supported 79% of all posterior loadings, and all of the anterior compressive loads. The LCL supported the anterior compressive loads and 21% of the posterior loads. The menisci transferred 62% of the total axial loads for anterior loads, 75% of the posterior loading, and 43% of the rotary loads.

An investigation on the interactions between ligaments and articular surfaces affected the motion of the passive knee joint has been reported in the literature. (Amiri, 2007) states that mechanism-based models that treat joint ligaments as bar linkages of a constant length, can

predict joint motion of an unloaded model, so this method was used. To generate the computer model, first the geometry of the knee joint was obtained from cadaveric knees, as in studies (Sugita and Amis, 2001), (Shelburne and Pandy, 1996) and (Li and Vandeveldi, 2008). It was mentioned in this particular study that, to obtain realistic results, the geometry of the model should be accurate. Five cadaveric knees were used in the generation of data for this model. The surface geometry, articular surface geometries, and insertion cites of the ligaments were taken from each knee. The contact points were recorded with the tibia fixed and the femur bent at 0˚, 30˚, 45˚, 90˚, and 120˚. To do this, pins were used as markers and their locations were recorded and later used for the production of the computer model. The bones were stripped of ligament tissue and scanned using PlyWorks software; to generate the remainder of the model SolidEdge software was used. The ligaments were represented by ligament bundles which act as nonlinear springs, and their slack length values were taken from literature such as (Akalan et al., 2008). To simulate wrapping, of the MCL around the tibia, each MCL bundle used in the model was modeled by two springs of equal lengths that were attached to each other. At their common end a spherical part was attached, the contact felt between the sphere and the medial side of the tibia. This was a good approximation of the wrapping effect. The model was run in a quasi-static mode with an initial flexion of 0˚ and a final flexion of 120˚ and 360 positions were recorded. At each position the resultant internal moments, and the anterior forces of each internal force was analyzed. The model was compared to others in literature and overall the model was in agreement with those previously reported. It was found that at 0˚ the ACL, LCL, and menisci horns contributed the most when it came to stabilizing the knee. From 0˚ to 30˚ there was a decrease of the internal forces in the cruciate ligaments. From 30˚ to 90˚ the tibial plateau and the LCL created forces that controlled rotation. From 90˚ to 120˚ there was a considerable amount of

contact between the medial condyle and the meniscus horn, the rotation was maintained by the cruciate ligaments. This is important in the design of total knee replacements.

A finite element model was used to analyze the response of the knee joint, particularly articular cartilage under external loadings that are associated with the standing position. According to (Vaziri, 2008), articular cartilage damage can be classified into two groups;

Type 1: Damage without affecting the bone or calcified cartilage, and

Type 2: Subcondylar fracture. The complexity of the structure complicates the development of theoretical and numerical models for analysis.

The cartilage can be subdivided into three sections the superficial layer, the middle layer and the calcified cartilage. In this study an axisymmetirc model was created, and three sets of numerical models were developed. In the first model, each layer was modeled as a single poroelastic isotropic layer, in the second model each layer was modeled as a single poroelastic transversely isotropic layer, and in the final model the superficial layer was modeled as transverse isotropic, the middle and calcified cartilage were considered as poroelastic and isotropic layers respectively. To analyze the effect of menisectomy on the knee joint and how the stress would be effected required a model of a knee with a healthy meniscus and one without the meniscus. The meniscus was modeled as a poroelastic transversely isotropic material, which allows the material to have higher stiffness in the circumferential direction. For the simulation a uniform pressure was applied to the bottom face of the tibia it started at 0 and increased to 0.17 MPa in 1s then remained constant for 60s. The articular damage is believed to derive from excessive shear stress so an analysis of the stress was presented. In all of the models an increase in shear stress was noticed after menisectomy, in one model the maximum shear stress increased by a factor of 5.

In recent years researchers have found an interest in in-vivo studies, (DeFrate, 2004) among others have developed methods to obtaining geometric data from MRIs, computed tomography scans, and fluoroscopic imaging techniques. (Bei, 2004) proposed an approach to sink deformable contact models with multi-body dynamic simulations to predict muscle forces, joint motion, and contact pressures simultaneously. The model was created using MRI and computed tomography scan information, as in past studies, the data was fed into computer-aided design software, to represent the contact in the model an accurate account of the geometry was calculated by a numerical integrator, in this case the tessellated surface approximation method. Once the contact surfaces were calculated, all the information was converted into an anatomical coordinate system. Now using the elastic contact theories the contact pressure was calculated, to simplify the model a "bed of springs" theory was used, which does not take into account how an applied pressure will affect surrounding areas, but does allow for faster pressure calculations. For small deformations in the knee equation was used to find the pressure, but in cases that involved larger deformations equation was used. Once the pressure for every element had been calculated the net forces were calculated. The force of each element was found and replaced by a force vector and the contact torque was calculated as well. This information was generated by a C++ program that used an ACIS 3D Toolkit to model the parameters listed above. Two simulations were conducted with this information to study the influence of contact pressures and material choices for the model. First, a static analysis was created, data from a single cadaveric knee was used to validate some of the strain calculations. The data was gathered using a GE LightSpeed QX/i scanner, the articular cartilage and subchondral bone surfaces were manually inputted from the MRI data, while cortical bone was surfaces were taken from computed tomography scans using a watershed algorithm. The data was merged with the information generated earlier into

Pro/MECHANICA MOTION to create a composite model that encompassed all of the necessary geometrical information with a tolerance of 0.18 mm for the femur and 0.29 mm for the tibia. During the simulation the femur was fixed at 30˚ of flexion and under 1000 N vertical load to allow for contact to occur. To account for the omitted meniscus and ligaments forces and stability contributions the remaining degrees of freedom were closely controlled to match data collected from other experiments. The dynamic simulation modeled an Osteonics 700 cruciate retaining knee implant, the geometry was modeled in computer-aided design software, and the contact surfaces were found then put into the model. This information was merged in Pro/MECHANICA MOTION and a multi body model was generated. External experiments were conducted to develop the parameters required as input information to allow for a successful simulation. Finally, the analysis was capable of predicting motion, contact force and torque. It was mentioned that the data generated was in agreement with expected data when it came to the damaged areas of the cartilage as well as the maximum amount of damage.

CHAPTER III

METHODOLOGY

In general, mathematical models are used for design, analysis and control purposes (Huss et al., 2000). Analysis is performed to determine stability and response of a system under a given condition. With the analysis, the design of the system can be altered and improved to achieve the desired state. In order to improve upon existing knee replacement technologies, the internal forces within the knee must be calculated based upon measurements taken from force plates and motion capture systems.

In this work, the goal is to use an inverse dynamics approach in order to determine the internal loads in the human knee during moderate squat exercise. This method is based upon motion captured coordinate data for the knee, ankle and hips as well as ground reaction forces along with their center of pressure of the ground reaction forces.

3.1. Dynamic Model

The present model of the human knee consists of two bony structures, namely femur and tibia, Figs. 3.1 and 3.2, respectively. One can notice that the knee is not modeled as a revolute joint. Since this model is used for walking and moderate squatting, both bones move. Between femur and tibia the ligamentous structure considered consists of the four major ligaments, namely ACL, PCL, MCL and LCL.

Although included in the model, *Fcx* is assumed to be zero, i.e. the friction between tibia and femur is neglected.

Each body has its own local coordinate system embedded in the body at it's the center of mass. The global coordinate system for the model is a fixed coordinate system XY, Fig 3.1.

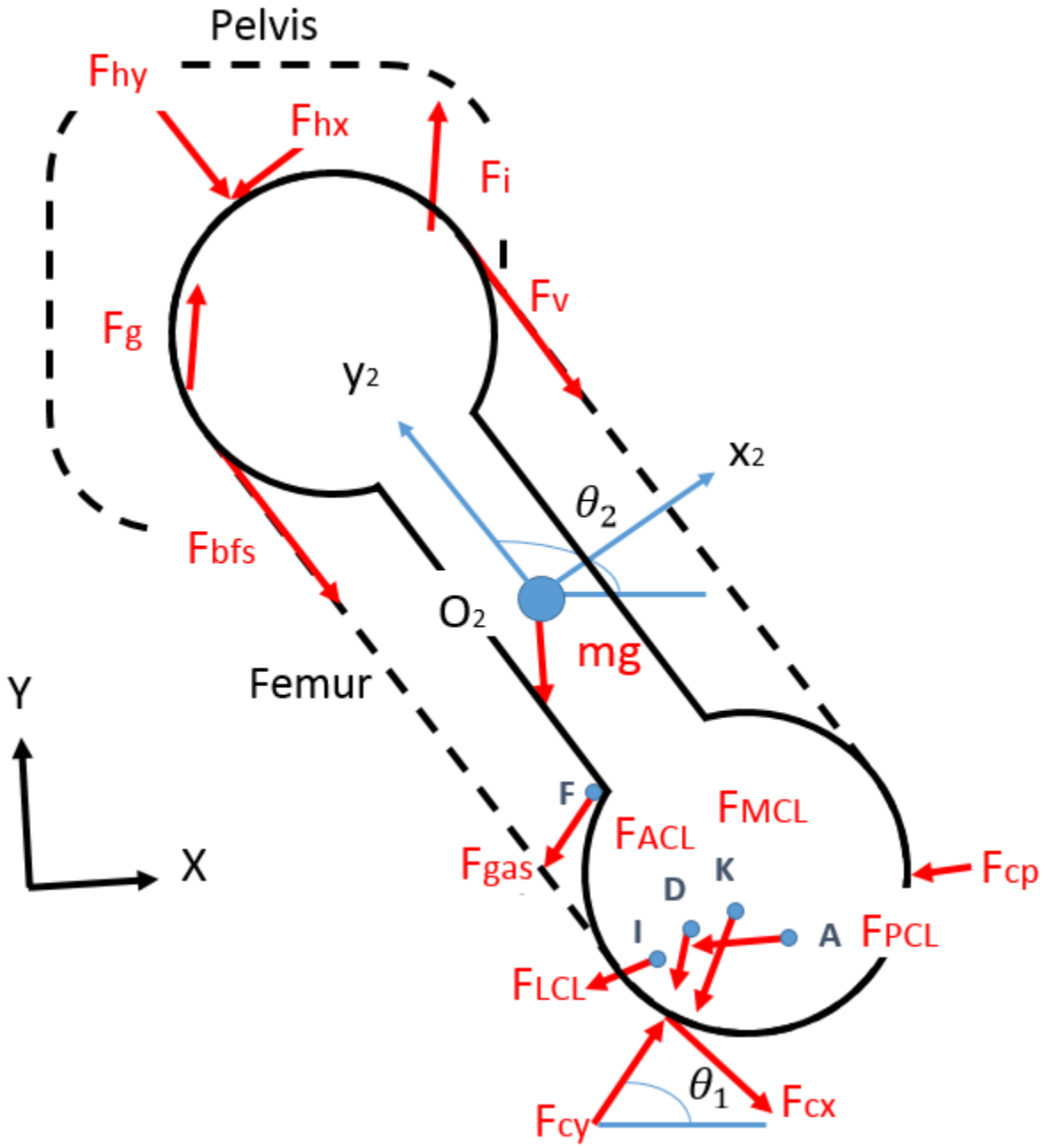

Figure 3.1 Free body diagram of femur.

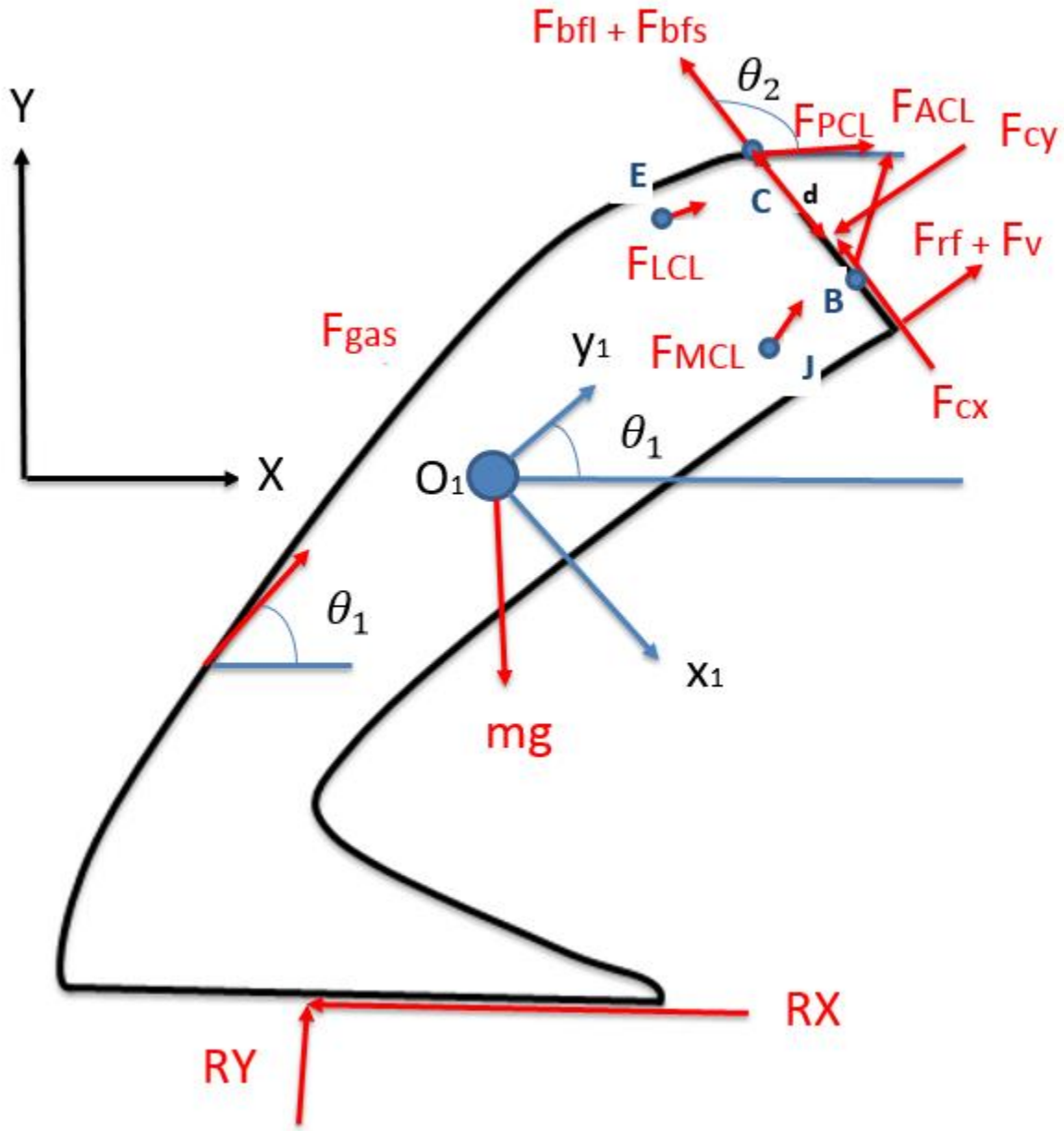

Figure 3.2 Free body diagram of tibia.

The forces in these ligaments are denoted by F_{acl}, F_{pcl}, F_{mcl} and F_{lcl} , Figs. 3.1 and 3.2. The muscles included in this model and their forces are as follows: 1) biceps femoris long head (F_{bfl}) between tibia (fibula head) and pelvis (ischial tuberosity), (2) biceps femoris short head (F_{bfs})

between tibia (fibula head) and femur (linea aspera and lateral supracondylar line of femur), (3) rectus femoris (F_{rf}) between pelvis (anterior inferior iliac spine) and patella (base), (4) vasti (F_v) (resultant of the vastus lateralis, vastus medialis and vastus intermedius) between femur and patella (base), (5) gastrocnemius (F_{gas}) between femur (condyles) and calcaneus (heel bone) through Achilles tendon, (6) gluteus medius (F_g) between pelvis posterior side (outer side of ilium, between iliac crest and posterior gluteal line) and femur (greater trochanter), and (7) iliacus (F_i) between pelvis anterior side (the region of the anterior inferior iliac spine) and femur (lesser trochanter). The hamstring muscle (F_h) is described by two groups of muscles, biceps femoris long head and biceps femoris short head as

$$F_h = F_{bfl} + F_{bfs} \tag{1}$$

The quadriceps muscle (F_q) is described by two groups of muscles, rectus femoris and resultant vasti as follows

$$F_q = F_{rf} + F_v \tag{2}$$

Also the contact forces in the knee and the hip are as follows: knee contact force on the tibial x_1 direction (F_{cx}), knee contact force on the tibial longitudinal y_1 direction (F_{cy}), hip contact force on the femoral x_2 direction (F_{hx}), and hip contact force on the femoral longitudinal y_2 direction (F_{hy}), Figs. 1 and 2.

This model also includes coordinates for the insertion points of the muscles, tendons and ligaments which includes ACL (x_D , y_D on femur and x_B , y_B on tibia), PCL (x_A , y_A on femur and x_C , y_C on tibia), LCL (x_I , y_I on femur and x_E , y_E on tibia), MCL (x_K , y_K

on femur and x_J , y_J on tibia), gastrocnemius (x_F , y_F), Fg (x_G , y_G), Fi (x_H , y_H). Mass is represented as m, acceleration in the x-direction a_x and acceleration in the y-direction a_y, gravity g, moment of the hip M_h, moment of the knee M_k, reaction at the foot in the x & y direction R_x and R_y, the tibia radius t_{rad}, the femur radius f_{rad}, the center of pressure cop_x, length of the tibia L_1 , the length of the femur L_2, the center of mass of the tibia in the x & y direction x_{com} & y_{com} and the center of mass of the femur in the x & y direction $x_{comthigh}$ and $y_{comthigh}$.

The assumptions made in this work are as follows:

1) The patellar tendon force acting on tibia is parallel to the longitudinal axis of tibia, and its magnitude equals the quadriceps force F_q given by Eq. (1). One can notice this investigation does not include patella.
2) F_{gas}, and F_{cy} are parallel to longitudinal axis of tibia, and F_{cx} perpendicular to this axis, i.e. parallel to the tibial plateau.
3) F_{bfs}, F_{bfl} and F_{hy} are parallel to femoral longitudinal axis, and F_{hx} perpendicular to it.

Each body has its own local coordinate system embedded in the body at it's the center of mass. The global coordinate system for the model is a fixed coordinate system, Fig. 3.1.

3.2. Dynamics Equations

The following are the equations which describe the 2-D leg dynamics, i.e. Newtons 2nd law along X and Y directions, and Euler equation along Z direction, Fig. 3.1.

For femur, Newtons 2nd law along X and Y directions,

$$\sum F_{Xf} = m_f \times a_{XCf} \tag{3}$$

$$\sum F_{Yf} = m_f \times a_{YCf} \tag{4}$$

and Euler equations (about the femoral center of mass).

$$\sum M_{Cf} = I_{Cf} \times \alpha_f \tag{5}$$

For tibia, Newtons 2nd Law along X and Y directions, Fig. 3.2,

$$\sum F_{Xt} = m_t \times a_{XCt} \tag{6}$$

$$\sum F_{Yt} = m_t \times a_{YCt} \tag{7}$$

and Euler equations (about the tibial center of mass).

$$\sum M_{Ct} = I_{Ct} \times \alpha_t \tag{8}$$

where F_{Xf}, F_{Yf}, M_{Cf} and $a_{XCf}, a_{YCf}, \alpha_f$ are the sum of forces and moments and their corresponding accelerations along X and Y axes, and with respect to the center of mass of femur around Z axis, respectively; and m_f, I_{Cf} the mass and the moment of inertia of femur; similarly for tibia. The moments of inertia of femur and tibia are found based on the anthropometric data. Based on the subject height, the segments' lengths and their radii of gyration are found (Winter, 2009), and consequently the moments of inertia calculated.

Explicitly the femoral equations are:

$$\left[F_{hy}+F_{bfs}+F_{v}\right]\times\cos\left[\theta_2+\pi\right]+F_{hx}\times\cos\left(\theta_2+\frac{\pi}{2}\right)+F_{gas}\times\cos\left(\theta_1+\pi\right)+F_{cy}\times\cos\left(\theta_1\right)-\left[\frac{F_{acl}\left(x_B-x_D\right)}{\sqrt{\left(x_B-x_D\right)^2+\left(y_B-y_D\right)^2}}\right]-$$
$$\left[\frac{F_{pcl}\left(x_C-x_A\right)}{\sqrt{\left(x_C-x_A\right)^2+\left(y_C-y_A\right)^2}}\right]-\left[\frac{F_{lcl}\left(x_E-x_I\right)}{\sqrt{\left(x_B-x_I\right)^2+\left(y_B-y_I\right)^2}}\right]-\left[\frac{F_{mcl}\left(x_J-x_K\right)}{\sqrt{\left(x_J-x_K\right)^2+\left(y_J-y_K\right)^2}}\right]+F_{cp}\times\cos\left(\beta+\pi\right)=m\times a_x=H_x$$

(9)

$$F_g+F_f+\left[F_{hy}+F_{bfs}+F_{v}\right]\sin\left(\theta_2+\pi\right)+F_{hx}\sin\left(\theta_2+\frac{\pi}{2}\right)+F_{gas}\sin\left(\theta_1+\pi\right)+F_{cy}\sin\left(\theta_1\right)-\left[\frac{F_{acl}\left(y_B-y_D\right)}{\sqrt{\left(x_B-x_D\right)^2+\left(y_B-y_D\right)^2}}\right]-$$
$$\left[\frac{F_{pcl}\left(y_C-y_A\right)}{\sqrt{\left(x_C-x_A\right)^2+\left(y_C-y_A\right)^2}}\right]-\left[\frac{F_{lcl}\left(y_E-y_I\right)}{\sqrt{\left(x_E-x_I\right)^2+\left(y_E-y_I\right)^2}}\right]-\left[\frac{F_{mcl}\left(y_J-y_K\right)}{\sqrt{\left(x_J-x_K\right)^2+\left(y_J-y_K\right)^2}}\right]+F_{cp}\sin\left(\beta+\pi\right)$$
$$=m\times a_y+m\times g=H_y$$

(10)

$$F_g\left(x_G-x_{comthigh}\right)+F_f\left(x_I-x_{comthigh}\right)+F_{hx}\times0.433\times segmentlengh2mean+\left(F_{bfs}-F_{v}\right)\times f_{rad}+$$
$$F_{gas}\left(x_F-x_{comthigh}\right)\sin\left(\theta_1+\pi\right)-\left(y_F-y_{comthigh}\right)\cos\left(\theta_1+\pi\right)+F_{cy}\times\left(x_4-x_{comthigh}\right)\times\sin\left(\theta_1\right)-\left(y_4-y_{comthigh}\right)\times\cos\left(\theta_1\right)+$$
$$\left[\frac{F_{acl}\left(x_B-x_D\right)}{\sqrt{\left(x_B-x_D\right)^2+\left(y_B-y_D\right)^2}}\right]\left[y_D-y_{comthigh}\right]-\left[\frac{F_{acl}\left(y_B-y_D\right)}{\sqrt{\left(x_B-x_D\right)^2+\left(y_B-y_D\right)^2}}\right]\left[x_D-x_{comthigh}\right]+$$
$$\left[\frac{F_{pcl}\left(x_C-x_A\right)}{\sqrt{\left(x_C-x_A\right)^2+\left(y_C-y_A\right)^2}}\right]\left[y_A-y_{comthigh}\right]-\left[\frac{F_{pcl}\left(y_C-y_A\right)}{\sqrt{\left(x_C-x_A\right)^2+\left(y_C-y_A\right)^2}}\right]\left[x_A-x_{comthigh}\right]+$$
$$\left[\frac{F_{lcl}\left(x_E-x_I\right)}{\sqrt{\left(x_E-x_I\right)^2+\left(y_E-y_I\right)^2}}\right]\left[y_I-y_{comthigh}\right]-\left[\frac{F_{lcl}\left(y_E-y_I\right)}{\sqrt{\left(x_E-x_I\right)^2+\left(y_E-y_I\right)^2}}\right]\left[x_I-x_{comthigh}\right]+$$
$$\left[\frac{F_{mcl}\left(x_J-x_K\right)}{\sqrt{\left(x_J-x_K\right)^2+\left(y_J-y_K\right)^2}}\right]\left[y_K-y_{comthigh}\right]-\left[\frac{F_{mcl}\left(y_J-y_K\right)}{\sqrt{\left(x_J-x_K\right)^2+\left(y_J-y_K\right)^2}}\right]\left[x_K-x_{comthigh}\right]+$$
$$F_{cp}\left(x_P-x_{comthigh}\right)\sin\left(\beta+\pi\right)-\left(y_P-y_{comthigh}\right)\cos\left(\beta+\pi\right)=I_{com2}\times\alpha_2=M_h$$

(11)

Explicitly the tibial equations are:

$$\left[F_{gas}-F_{cy}\right]\cos(\theta_1)+\left(F_{bfl}+F_{bfs}\right)\cos(\theta_2)+\left[\left(F_{rf}+F_v\right)\times\frac{\left(x_M-x_N\right)}{\sqrt{\left(y_M-y_N\right)^2+\left(x_M-x_N\right)^2}}\right]$$
$$+\left[\frac{F_{pcl}\left(x_A-x_C\right)}{\sqrt{\left(x_A-x_C\right)^2+\left(y_A-y_C\right)^2}}\right]-\left[\frac{F_{acl}\left(x_D-x_B\right)}{\sqrt{\left(x_D-x_B\right)^2+\left(y_D-y_B\right)^2}}\right]+ \tag{12}$$
$$\left[\frac{F_{lcl}\left(x_I-x_E\right)}{\sqrt{\left(x_I-x_E\right)^2+\left(y_I-y_E\right)^2}}\right]-\left[\frac{F_{mcl}\left(x_J-x_K\right)}{\sqrt{\left(x_J-x_K\right)^2+\left(y_J-y_K\right)^2}}\right]=m\times a_x+R_x=K_x$$

$$\left[F_{gas}-F_{cy}\right]\sin(\theta_1)+\left[F_{bfl}+F_{bfs}\right]\sin(\theta_2)+\left[\left(F_{rf}+F_v\right)\times\frac{\left(y_M-y_N\right)}{\sqrt{\left(y_M-y_N\right)^2+\left(x_M-x_N\right)^2}}\right]+$$
$$\left[\frac{F_{pcl}\left(y_A-y_C\right)}{\sqrt{\left(x_A-x_C\right)^2+\left(y_A-y_C\right)^2}}\right]+\left[\frac{F_{acl}\left(y_D-y_B\right)}{\sqrt{\left(x_D-x_B\right)^2+\left(y_D-y_B\right)^2}}\right]+ \tag{13}$$
$$\left[\frac{F_{lcl}\left(y_I-y_E\right)}{\sqrt{\left(x_I-x_E\right)^2+\left(y_I-y_E\right)^2}}\right]+\left[\frac{F_{mcl}\left(y_J-y_K\right)}{\sqrt{\left(x_J-x_K\right)^2+\left(y_J-y_K\right)^2}}\right]=m\times a_y-R_y+m\times g=K_y$$

$$-F_{gas}\times 0.03+F_{cy}\left(t_{rad}-d\right)+\left(F_{bfl}+F_{bfs}\right)\left[\left(x_C-x_{com}\right)\sin(\theta_2)-\left(y_C-y_{com}\right)\cos(\theta_2)\right]+$$
$$\left[\left(F_{rf}+F_v\right)\times\frac{\left(y_M-y_N\right)}{\sqrt{\left(y_M-y_N\right)^2+\left(x_M-x_N\right)^2}}\right]\left(x_N-x_{com}\right)-\left[\left(F_{rf}+F_v\right)\times\frac{\left(x_M-x_N\right)}{\sqrt{\left(y_M-y_N\right)^2+\left(x_M-x_N\right)^2}}\right]\left(y_N-y_{com}\right)+$$
$$\left[\frac{F_{pcl}\left(y_A-y_C\right)}{\sqrt{\left(x_A-x_C\right)^2+\left(y_A-y_C\right)^2}}\right]\left[x_C-x_{com}\right]-\left[\frac{F_{pcl}\left(x_A-x_C\right)}{\sqrt{\left(x_A-x_C\right)^2+\left(y_A-y_C\right)^2}}\right]\left[y_C-y_{com}\right]+$$
$$\left[\frac{F_{acl}\left(y_D-y_B\right)}{\sqrt{\left(x_D-x_B\right)^2+\left(y_D-y_B\right)^2}}\right]\left[x_B-x_{com}\right]-\left[\frac{F_{acl}\left(x_D-x_B\right)}{\sqrt{\left(x_D-x_B\right)^2+\left(y_D-y_B\right)^2}}\right]\left[y_B-y_{com}\right]+$$
$$\left[\frac{F_{lcl}\left(y_I-y_E\right)}{\sqrt{\left(x_I-x_E\right)^2+\left(y_I-y_E\right)^2}}\right]\left[x_E-x_{com}\right]-\left[\frac{F_{lcl}\left(x_I-x_E\right)}{\sqrt{\left(x_I-x_E\right)^2+\left(y_I-y_E\right)^2}}\right]\left[y_E-y_{com}\right]+$$
$$\left[\frac{F_{mcl}\left(y_K-y_J\right)}{\sqrt{\left(x_K-x_J\right)^2+\left(y_K-y_J\right)^2}}\right]\left[x_J-x_{com}\right]-\left[\frac{F_{mcl}\left(x_K-x_J\right)}{\sqrt{\left(x_K-x_J\right)^2+\left(y_K-y_J\right)^2}}\right]\left[y_J-y_{com}\right]$$
$$=\left[I_{com}\times\alpha\right]+\left[R_x\times 0.394L_1\right]-\left[R_y\times\left(copx-x_{com}\right)\right]=M_k$$

(14)

3.3. Inverse Dynamics Model

The dynamic model consists of 6 second-order differential equations. The 6 accelerations and the 2 ground reaction forces are given by experimental data collected using a motion analysis system and force plates available in the Biomechanics Laboratory at UTPA. This data is used as input data for the inverse dynamics model. The unknowns of the system are 4 ligamentous forces, 4 contact forces, 9 muscle forces, and the distance (*d*) between the back of the tibial plateau and the tibio-femoral contact point. Since the number of unknowns is larger than the number of equations, inverse dynamics (optimization) is used in this work. Optimization approach is a method for finding a unique best solution among the infinite number of solutions of such systems (with more unknowns than equations available).

The inverse dynamics model is an optimization in which a) the equality constraints are given by Eqs. (9-14), and b) the inequality constraints consist of all forces in ligaments and muscles being positive (only tension). Distance *d* is assumed to be between 0 and .05 meters. c) The objective function of the optimization in this work is to minimize the sum of squares of all forces of the model.

3.4. Experimental Data

The body movement and ground reaction forces were captured using a motion analysis system and force plates, see section 4.2.1. Motion capture is the process of recording the movement of objects or subjects. In many fields, motion capture is sometimes called motion tracking. One technique for developing information on the kinematics of the knee joint involves reflective markers which act as nodes that are attached to the skin and sometimes directly to the bone. The markers are monitored by multiple video cameras that can generate a three-dimensional marker trajectories. The reflective markers that are attached to the bone eliminate

any error in motion due to the motion of the skin over the knee joint (Li and Vandeveldi, 2008). In motion capture sessions, movements are usually sampled at a rate of 100 times per second. Whereas early techniques used images from multiple cameras to calculate positions of different body parts, often the purpose of motion capture is to record only the movements of the subject, not the visual appearance (Bendjaballah et al., 1995).

3.5. Method of Optimization

The method of optimization used in MATLAB is using fmincon, which finds the minimum of constrained nonlinear multivariable function. The optimization of the knee was using experimental values that were obtained by using the Nexus software in the Biomechanics lab at The University of Texas – Pan American. The data was extracted and then put on an excel spreadsheet where the data was then filtered out using an m-file on Matlab by using polyfit. This polyfit equation was then put in the Matlab code and the same simulations were done with data obtained from the experiment.

The results that were generated are accurate to how the model should behave. This is good for future utilization of both the Nexus technology and the Matlab code that is generating good results.

The optimization uses five m-files. Each one serves a specific purpose and was separated so that simple alterations could be made without adjusting the entire code. From experiment to experiment, it may be necessary to alter certain parameters. The five Matlab codes and their descriptions are listed below.

- *Main*

  The Matlab code "*Main*" is used to execute the optimization process and calls all the other m-files as needed. It utilizes the Matlab optimization function "*fmincon*."

"*Fmincon"* minimizes the forces in the knee. The optimized forces such as *Fh*, *Fq*, *Fcx, Fcy,* and distance *d* are then plotted.

- *MultiplePointsDataMatrix*

  The Matlab code "*MultiplePointsDataMatrix*" is used to provide raw or filtered data to "*Main*". The data included are: frame number, time of data point collection, *x* and *y* coordinates of the knee and ankle, and the *x* and *y* ground reaction forces. Filtered data is to be used.

  ***** Note: If a reduced section of data is to be analyzed (ex. just a section with ground forces), then the unused data points should be removed from the m-file before being forwarded on to "*Main.*"

- *multiplepoints*

  The Matlab code "*multiplepoints*" is used to perform calculations on the filtered data to arrive at values that can be used in the optimization process. With coordinate data for the knee and ankle, the velocities (*x, y,* rotational) and the accelerations (*x, y,* rotational) can be calculated. Necessary anthropometric data can also be calculated such as the leg segment length, the subject height, radius of gyration and the moment of inertia. All of these calculations, combined with the ground reaction forces (*Rx* and *Ry*) and inertial forces are to be used in the constraints file mycon.

- *mycon*

  The Matlab code "*mycon*" is used to set up the equality and inequality constraints of the optimization process. The equality constraints are given by Eqs. (9-14). The

inequalities assume that the forces are greater than 0 Newtons. They also assume that the distance "*d*" must be greater than 0 meters but less than 0.05 meters.

- *kneefunction*

  The Matlab code "*kneefunction*" provides an objective equation that sums the squares of the 16 unknown variables with the exception of the distance "*d*". It is not necessary for "*d* " to be minimized.

The inequality constraints are as follows:

$F_{bfl} > 0$ Biceps femoris long head

$F_{rf} > 0$ Rectus femoris

$F_{cx} = 0$ Contact force knee

$F_{cy} > 0$ Contact force knee

$0 < d < 0.03$ Distance

$F_{g} > 0$ Gluteus

$F_{i} > 0$ Iliacus

$F_{hx} > 0$ Contact force hip

$F_{hy} > 0$ Contact force hip

$F_{v} > 0$ Vasti

$F_{bfs} > 0$ Biceps femoris short head

$F_{acl} > 0$ ACL

$F_{pcl} > 0$ PCL

$F_{gas} > 0$ Gastrocnemius

$F_{lcl} > 0$ LCL

$F_{mcl} > 0$ MCL

The objective function in this work is to minimize the forces in muscles, ligaments and contact forces. There are other objective functions proposed in the literature based on various physical grounds (Bartel et al., 2006).

$$F = F_{bfl}^{\ 2} + F_{rf}^{\ 2} + F_{cy}^{\ 2} + F_{q}^{\ 2} + F_{f}^{\ 2} + F_{hx}^{\ 2} + F_{hy}^{\ 2} + F_{v}^{\ 2} + F_{bfs}^{\ 2} + F_{ACL}^{\ 2} + F_{PCL}^{\ 2} + F_{gas}^{\ 2} + F_{LCL}^{\ 2} + F_{MCL}^{\ 2} \quad (13)$$

CHAPTER IV

EXPERIMENTAL PROTOCOL

This chapter describes how the data was collected from the experimental work. All tests and subsequent analysis were conducted under strict guidelines to insure the validity of data and avoid extraneous factors that may have skewed the data collected.

4.1. Procedures for Squat Motion

4.1.1.Warm-up and Practice

Before conduction the actual data recording, the subject would perform a self-selected warm-up. When the warm-up was completed, the subject was required to complete a practice of ten squat repetitions. After the ten warm-up repetitions, the subject was required to rest for ten minutes to avoid the onset of muscle fatigue during testing and to confirm that the subject was using proper technique.

4.1.2. Testing and Subject Preparation

Upon the completion of the practice set, the subject began the testing protocol of beginning to complete ten repetitions of squats followed by ten minutes rest time, then doing another ten repetitions for a total of ten trials. This means that a total of 100 squats were done, but in sets of ten repetitions with ten minutes of rest in between each trial. Also, the subject was required to hold their arms straight forward and stand erect during each repetition.

Reflective markers were placed on various landmarks on the subject. The objective is to get the markers to move as close as possible to the bone. The reflective markers were placed on the toe, heel, the lateral knee, the medial knee, the side hip, the front torso and the rear torso. As shown in Fig. 4.1. Shells were also place on the foot, shin and the thigh. These shells are useful when the recorded data for the trajectories has gaps due to the fact that the marker may have been covered during the movement. These shells help the program guess where the marker actually was during the motion and will manually have to be re-labeled to the correct marker.

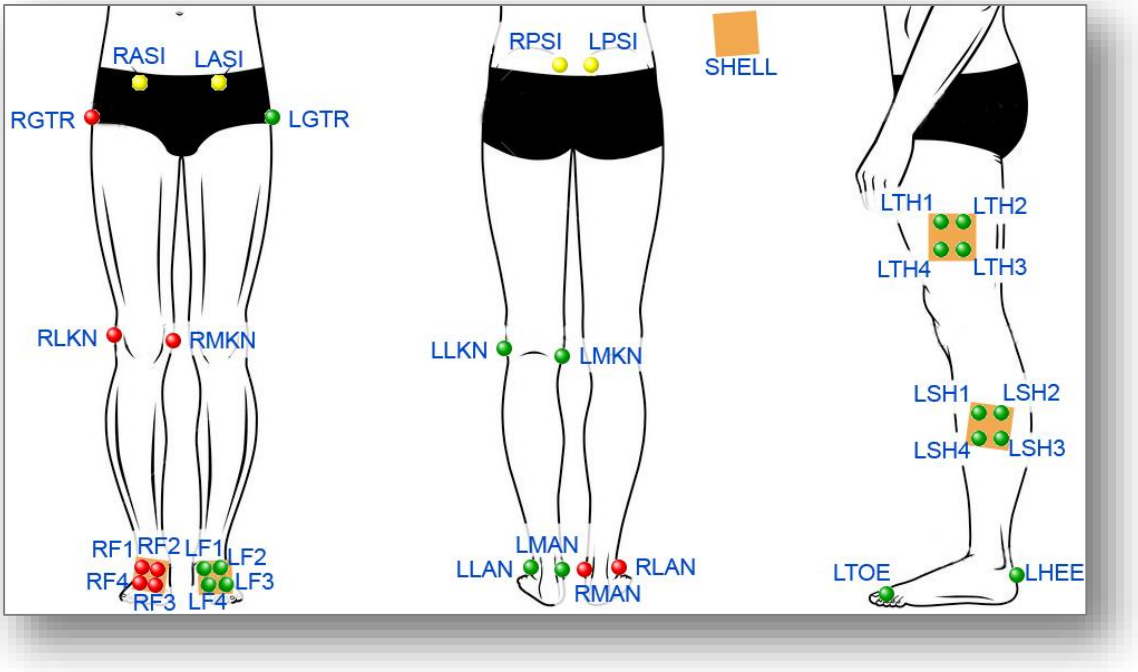

Figure 4.1 Location of reflective markers on lower body.

4.1.3. Technique

Proper execution of each trial is important to eliminate other extraneous variables that may skew the collected data. Each participant was instructed to maintain an erect posture and avoid the knee projecting in front of the toes. The subject were required to execute a parallel

squat for each trial taken while standing with both feet each on a different force platform. A parallel squat (or moderate squat) was defined as the approximate location of the femur (midway between the top and the bottom of the thigh) being parallel to the floor. The subject descends until the upper thigh is parallel to the floor while the heels remain in contact with the floor the entire time and the knees crossing the vertical plane of the toes as little as possible, if at all. The upper body remains as still as possible with chest out and the eyes looking forward or slightly up. The hips are lowered as if sitting in a chair and at the lowest point the center of pressure (COP) is over the heel or arch of the foot. The subject then begins to ascend, extending the knees, hips, and ankle until they are again standing erect in the starting position. Trials were discarded if a participant's feet do not remain flat on the force platform or if they fail to reach parallel. Each repetition for each trial was executed at a self-selected pace.

Figure 4.2 Starting position of squat.

Figure 4.3 Example of lowest point during traditional squat.

Figure 4.4 Lowest point during moderate squat sagittal view.

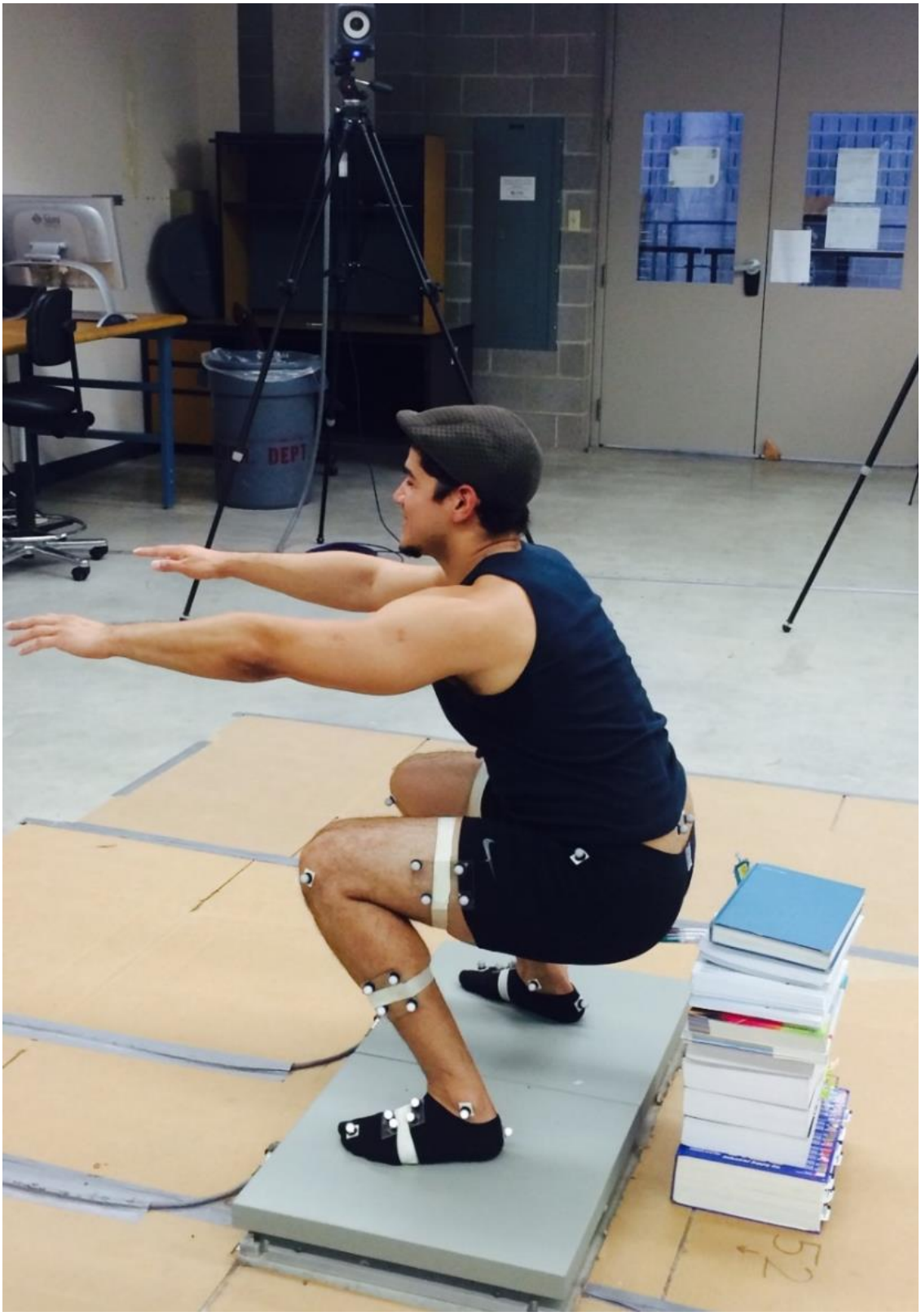

Figure 4.5 Another view of moderate squat .

4.2. Data Collection

4.2.1. Force Platform

An AMTI force plate is used in this study which is designed to measure ground reaction forces and the center of pressure applied to their top surface. The force plate is used with a sampling at 1000 Hz was used to collect ground reaction force (GRF) data as well as the force displacement throughout the participant's foot. The force plate data was also used for the calculation of the forces at the knee, hip and ankle. The size of the top surface of the force platform 0.6m x 0.6m as shown in Fig. 4.6.

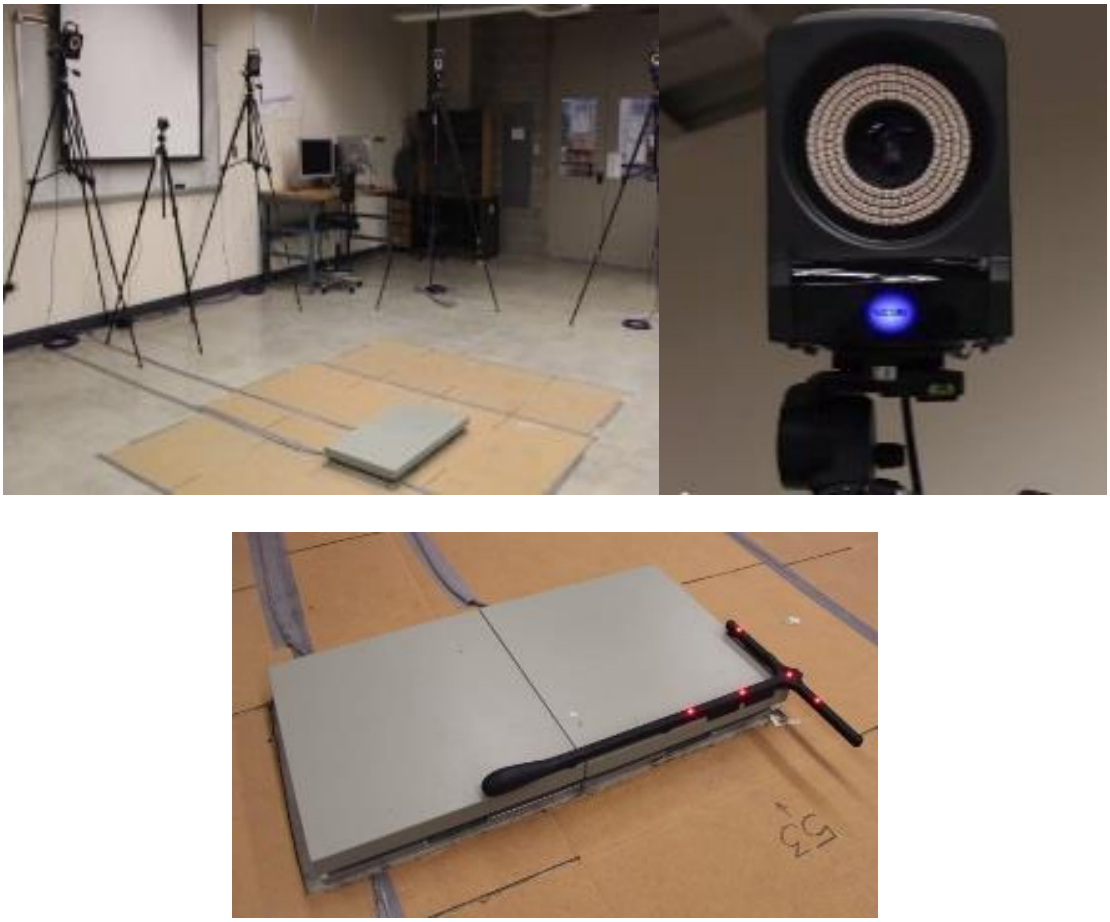

Figure 4.6 Biomechanics Laboratory at UTPA, NSF grant (Left), Vicon Motion Analysis System camera (Middle), and Force Plates (Right).

4.2.2. Videography

Reflective markers were placed on sites of the hip, thigh, knee, ankle, foot and torso to analyze squatting kinematics and kinetics using the Vicon motion system. Ten Vicon MX T-Series cameras with a sampling rate of 100 Hz were used to collect all the reflective marker position data. These cameras work by emitting light and capturing the reflections of those lights on the reflective markers. The subject performed a series of motions that allowed the Vicon motion system to identify the participant's hips and knees. Each camera was strategically positioned along the walls of the Biomechanics laboratory to allow for full view of all passive reflective markers as shown in Fig. 4.7. This eliminated any error due to estimation of reflective marker location during the execution of a trial. All this motion captured data was processed afterwards. The motion was also recorded by a Bonita HD camera, which captures images like a regular camera. It is a high-definition camera that recorded the subject from a frontal position in this exercise.

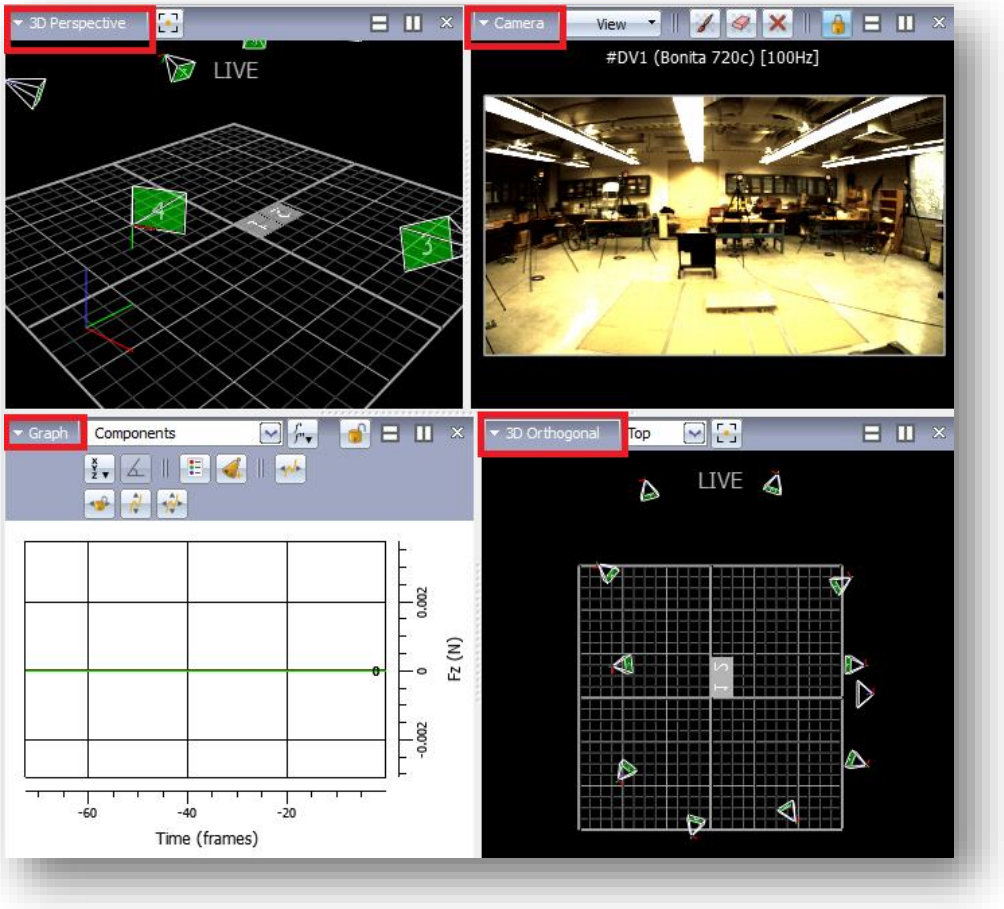

Figure 4.7 The ten Vicon MX T-Series cameras positioned in the Biomechanics laboratory.

4.2.3. Data Analysis

All this motion captured data was collected and processed by the Giganet, which is a part of the system that converts and carries all the analog and video data simultaneously into the computer so that it can be managed in the Vicon Nexus software. Once the all data is in the Vicon Nexus software, it is then exported to an excel spreadsheet where all the positions of the markers, the forces on the force plates as well as the center of pressure on the forces plates can be seen and analyzed.

The data collected was input into a 2D model through which kinematic and kinetic data were calculated. The Kinematic data was analyzed and post processed via a custom Matlab program.

4.2.4. Data Filtering

All the data gathered from the positions of the reflective markers was filtered by using regression to determine a proper fitting curve that fit the data. An equation was then obtained from the curve that fit the data and then input into the Matlab code for optimization.

CHAPTER V

RESULTS

In this section two exercises are investigated using the inverse dynamic model of this work. The first one is the gait exercise with experimental data from (Winter, 2009). The experimental data for the moderate squat exercise resulted from the experiments conducted in the Biomechanics Laboratory at UTPA. The inverse dynamics model data is then The inverse dynamic model data in both cases are compared with data available in the literature.

5.1. Gait Numerical Simulations – Validation of the Model

The simulations for gait cycle are presented next. The subject's flexion angle and ground reactions forces can be seen in Figs. 5.1 and 5.2, respectively. The pattern and the values of the flexion angle resulting from (Winter, 2009) in Fig. 5.1 are in agreement with data reported in the literature (Shelburne et al., 2004). The ground reaction forces (GRFs) from (Winter,2009) show an increase during the heel strike up to 600 N, then a decrease, an increase again up to 600 N and a decrease to zero during the toe off. This is in agreement with (Winiarski, 2009). GRF data is then used to help find the other forces in the muscles and the ligaments.

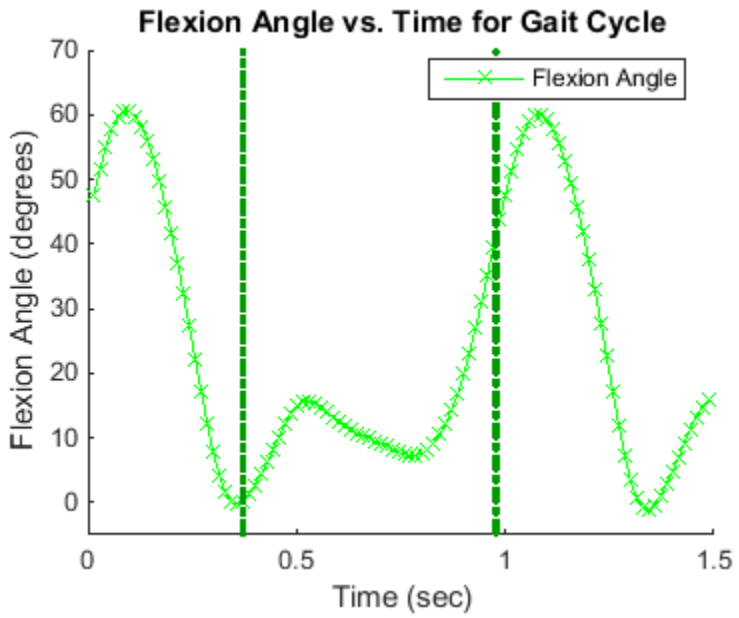

Figure 5.1 Flexion angle vs. time for gait cycle. The first vertical line represents heel strike and the second vertical line represents toe off. This data is from (Winter, 2009).

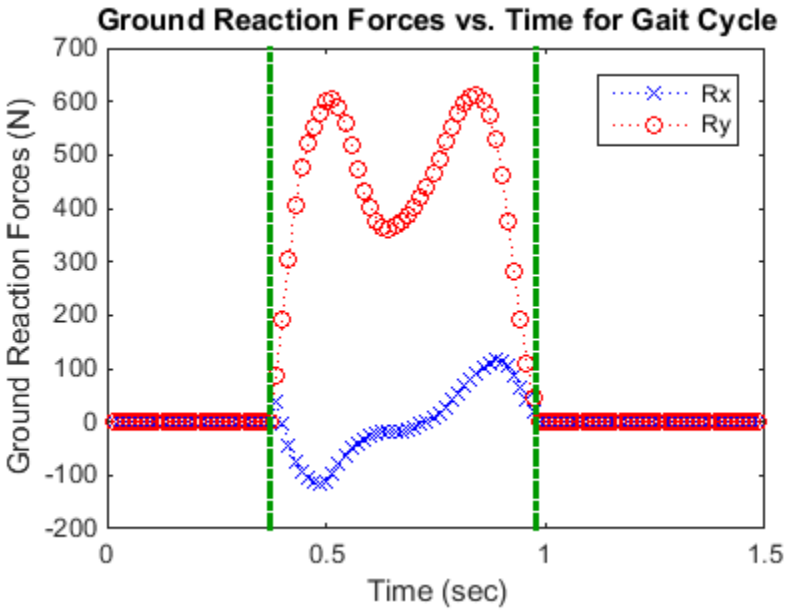

Figure 5.2 Ground reaction forces during gait cycle. The first vertical line represents heel strike and the second vertical line represents toe off. This data is from (Winter, 2009).

Fig. 5.3 illustrates the contact force location on the tibial plateau. The distance between the posterior side of the tibial plateau and the location of the contact point is denoted by *d*. It can be seen that the contact point is moving across the tibial plateau. After the heel strike, the contact point moves from 5 cm to 0 cm and then at 50% stance phase of gait, the contact force is at about 2 cm from the posterior side of the tibial plateau. Then at about 90% stance phase of the gait cycle, the contact force moves back to the posterior side of the tibial plateau. Fig. 5.3 shows *d* has a similar pattern and is in good agreement with what is found in (Mukoyama, et al., 2012).

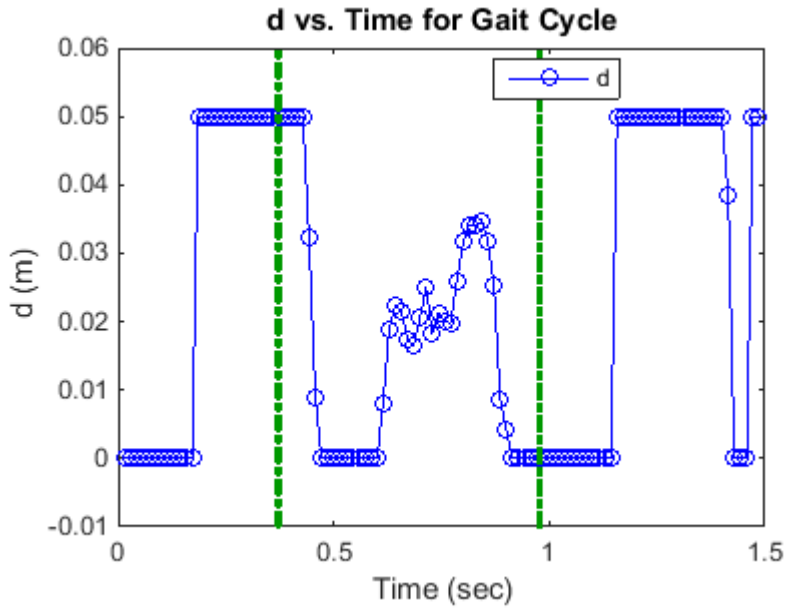

Figure 5.3 Distance *d* between posterior tibial plateau and contact point; 0< *d* <5 cm constraint. The vertical lines represent heel strike and toe off, respectively; (present work)

5.1.1. Ligament Forces

The results of this work show that ACL has two peaks during the first 40% of the stance phase which reach to about 200 N, then 300 N, and then the ACL force decreases to 0 N. From 40% to 90% of the stance phase, the ACL shows 0 N force applied before it hits 90% stance phase, and then shows another peak that reaches to about 130 N. The data obtained shows a good

agreement with other published work which show patterns of activity in the ACL of about 300 N at about 30% stance phase and then the ACL force slowly decreases, Fig. 5.4. Studies such as (Markolf et al., 1995), show that the ACL forces are higher when the leg tends to be fully extended.

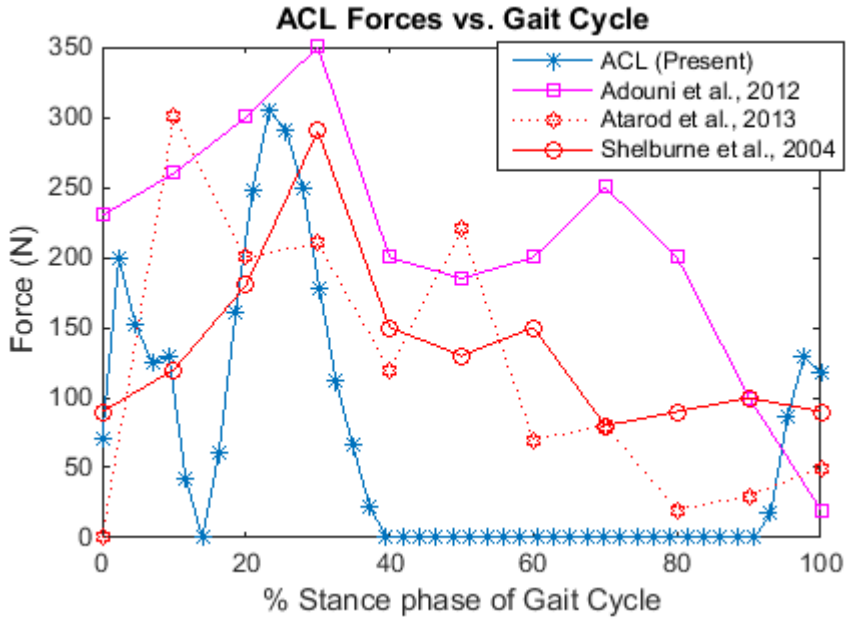

Figure 5.4 Anterior cruciate ligament force compared with other results. With 0% of stance phase representing heel strike and 100% stance phase representing toe off compared with (Adouni et al., 2012), (Atarod et al., 2013) and (Shelburne et al., 2004).

When comparing PCL forces of the present model with (Shelburne et al., 2004) Fig. 5.5, they are in agreement. They are in good agreement for half of the gait cycle. For the other half of the gait cycle although the forces predicted by this work are rather small, there are some differences. The differences are between 10% to 50% of the stance phase where this work predicts forces in PCL with a peak of about 230 N while (Shelburne et al., 2004) predicts no PCL force, and in the last 10% where this work predicts forces in PCL with a peak of about 70 N while (Shelburne et al., 2004) predicts no PCL force.

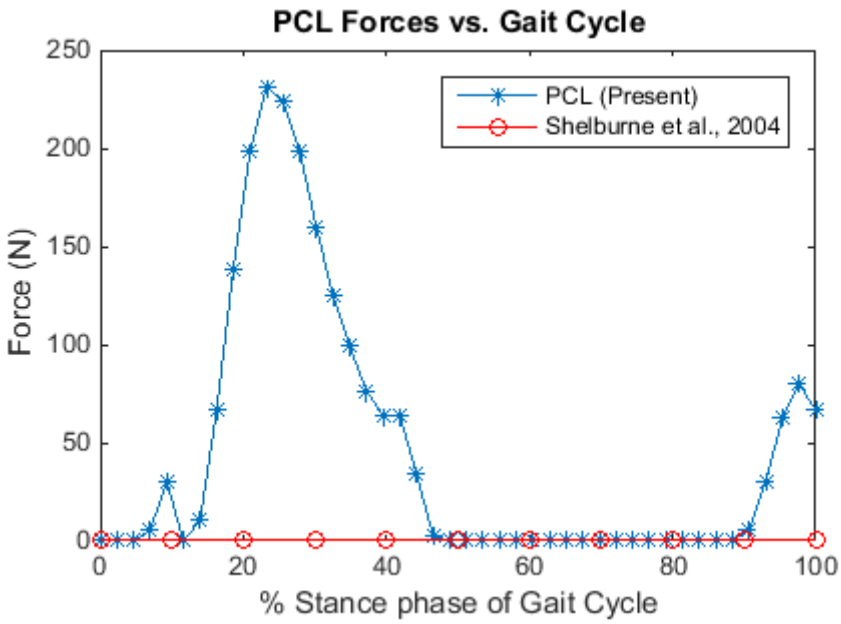

Figure 5.5 Posterior cruciate ligament force compared with other results. With 0% of stance phase representing heel strike and 100% stance phase representing toe off compared with (Shelburne et al., 2004).

Figure 5.6 shows that the LCL forces reaching a peak force of up to about 400N are slightly greater when compared to the ACL forces during the stance phase. From 0% to 40% stance phase the LCL does not show activity and then at 40% stance phase the LCL starts to show a steady increase of force until 80% stance phase, and then this force decreases to about 110N around 90% of the stance phase. The result of the force in the LCL shows a similar pattern as shown by (Adouni et al., 2012), which shows activity in the LCL during from 70% to 100% of the stance phase of the gait cycle. All works show LCL activity in the last half of the cycle.

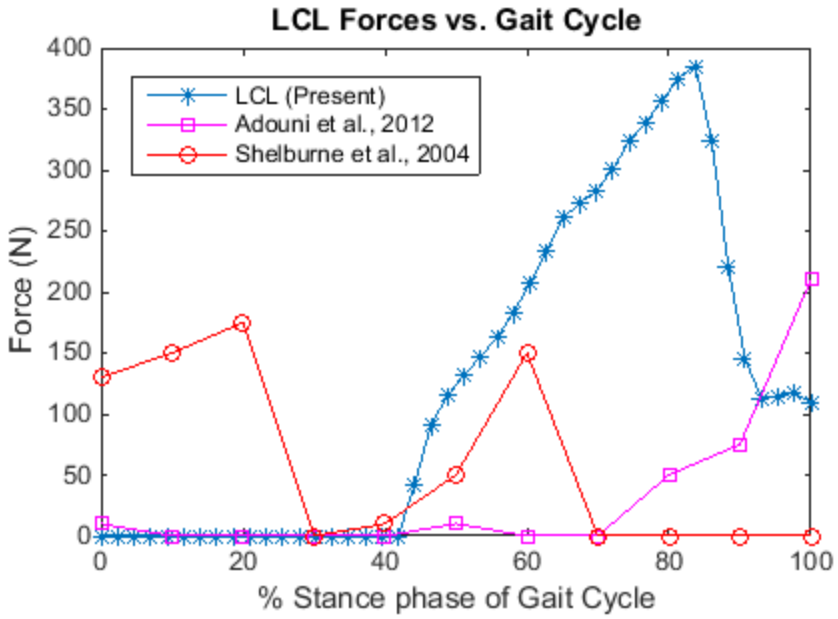

Figure 5.6 Lateral collateral ligament force compared with other results. With 0% of stance phase representing heel strike and 100% stance phase representing toe off compared with (Adouni et al., 2012) and (Shelburne et al., 2004).

Figure 5.7 shows predictions of little activity in the MCL at 10% of stance phase with the MCL force reaching about 10 N. After 10% stance phase, there is no activity in the MCL until about 90% of the stance phase when the MCL shows a force of up to about 155 N. There is a good agreement with data reported in the literature. Other works do not show much activity in the MCL either during the stance phase. (Adouni et al., 2012) does show a force of up to about 55 N during the first 20% of the stance phase and then does not show any more activity for the rest of the stance phase of the gait cycle.

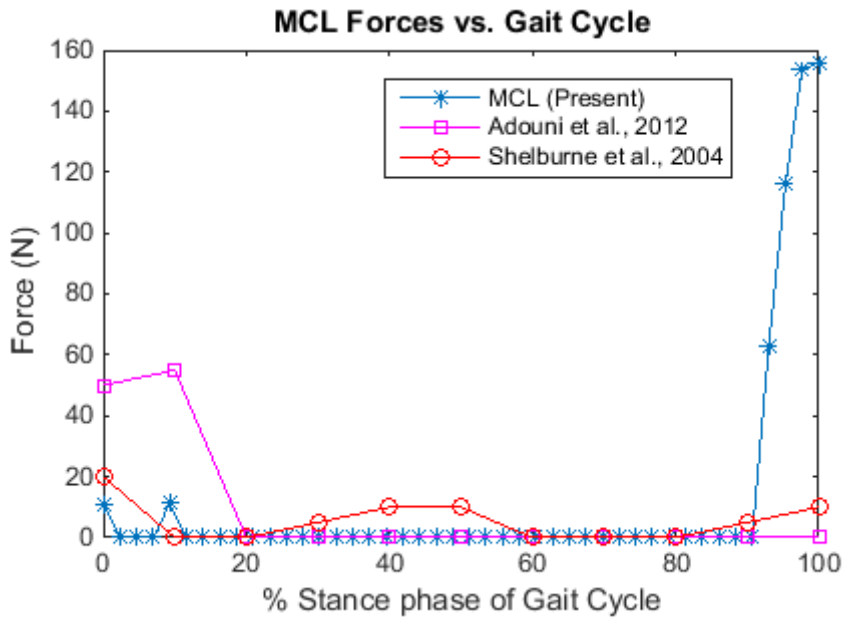

Figure 5.7 Medial collateral ligament force compared with other results. With 0% of stance phase representing heel strike and 100% stance phase representing toe off compared with (Adouni et al., 2012) and (Shelburne et al., 2004).

5.1.2. Muscle Forces

Figure 5.8 illustrates the quadriceps forces during the stance phase. This work predicts that from 0% to 40% of the stance phase, there is activity in the quadriceps muscle with forces reaching up to about 100 N. The force then decreases to 0 N at 40% stance phase where it continues to remain at 0 N until the subject reaches about 65% of the stance phase, where the force increases to about 400 N. Other work such as (Shelburne et al., 2004) and (Ping Lim et al., 2013), show the quadriceps force reaching a force of 1000 N at about 20% to 30% of the stance phase, the force then decreases to about 200 N, and then increases again of up to about 600 N at 100% of the stance phase of the gait cycle. All works show an increased activity of the quadriceps muscle in the first 40% and the last 30% of the gait cycle.

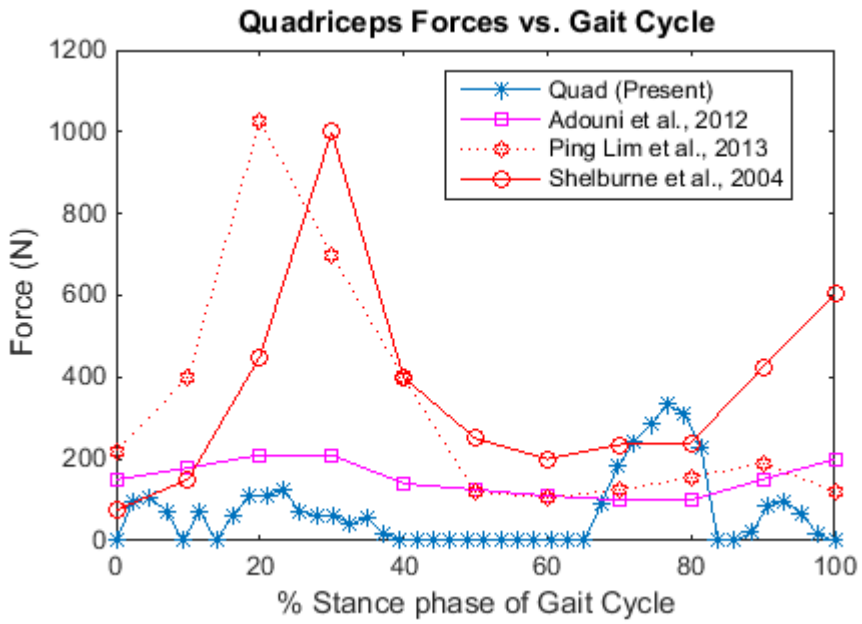

Figure 5.8 Quadriceps forces compared with other results. With 0% of stance phase representing heel strike and 100% stance phase representing toe off compared with (Adouni et al., 2012), (Ping Lim et al., 2013) and (Shelburne et al., 2004).

Figure 5.9 shows that the hamstring muscle is activated from 0% to about 10% of the stance phase, reaching a peak of up to about 460 N, then the hamstring force decreases to 0 N from 10% to about 45% of the stance phase. Once the hamstring is at about 45% of the stance phase, the force shown in the muscle increases to about 450 N then force starts to decrease to 0 N at 90% of the stance phase. Other work such as (Shelburne et al., 2004), showed the hamstring muscle having a force of about 250 N then steadily decreasing to 0 N when 100% of stance phase is reached. (Ping Lim et al., 2013) showed a peak force in the hamstring which reaches about 800 N at around 10% stance phase of the gait cycle before it then decreases to about 80 N at 100% of the stance phase. All works show higher level of activity in the first 10% of the gait cycle.

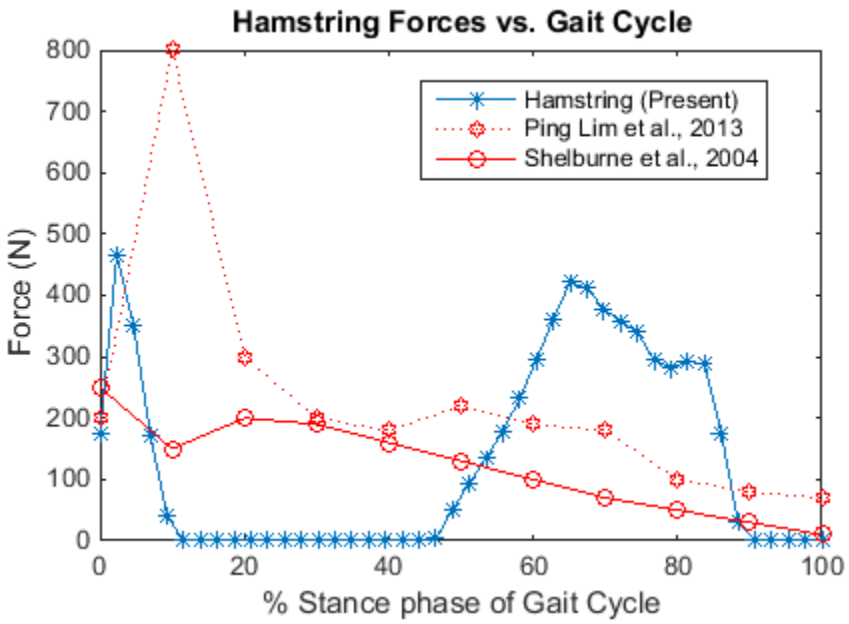

Figure 5.9 Hamstring forces compared with other results. With 0% of stance phase representing heel strike and 100% stance phase representing toe off compared with (Ping Lim et al., 2013) and (Shelburne et al., 2004).

Figure 5.10 shows the gastrocnemius, another important muscle during the gait cycle, is activated during the toe off phase. Most results according to other results seen show activity towards about 70% to 80% stance phase of the gait cycle. However, the results of this work showed activity in the gastrocnemius muscle reaching a force of up to about 200 N from 0% to about 10% of the stance phase and then did not show any activity from 10% to 80% of the stance phase of the gait cycle before increasing again to about 200 N during the toe off phase. All works show higher activity at the beginning of the stance phase and in the last 40%. The peak values of this work are in agreement with (Adouni et al., 2012), and the pattern with the other three works.

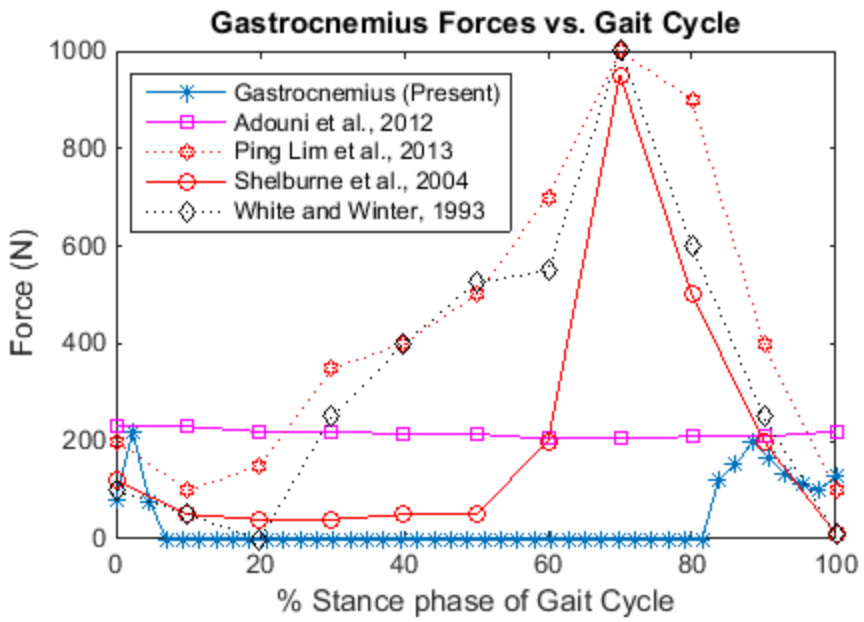

Figure 5.10 Gastrocnemius forces compared with other results. With 0% of stance phase representing heel strike and 100% stance phase representing toe off compared with (Adouni et al., 2012), (Ping Lim et al., 2013), (Shelburne et al., 2004) and (White and Winter, 1993).

Figure 5.11 shows the knee moment predicted for the gait cycle. During heel strike the moment increases from -18 Nm up to 18 Nm at about 20% the stance phase of gait, this point of 18 Nm is where the knee moment will reach peak and then the moment decreases to about -20 Nm at 50% the stance phase of gait and then the moment decreases to reach the negative peak of -60 Nm at about 80% of the stance phase at which the moment now will increase to about 0 Nm at 100% the stance phase of the gait cycle. The pattern of the knee moment is in good agreement with (Thambyah, 2008).

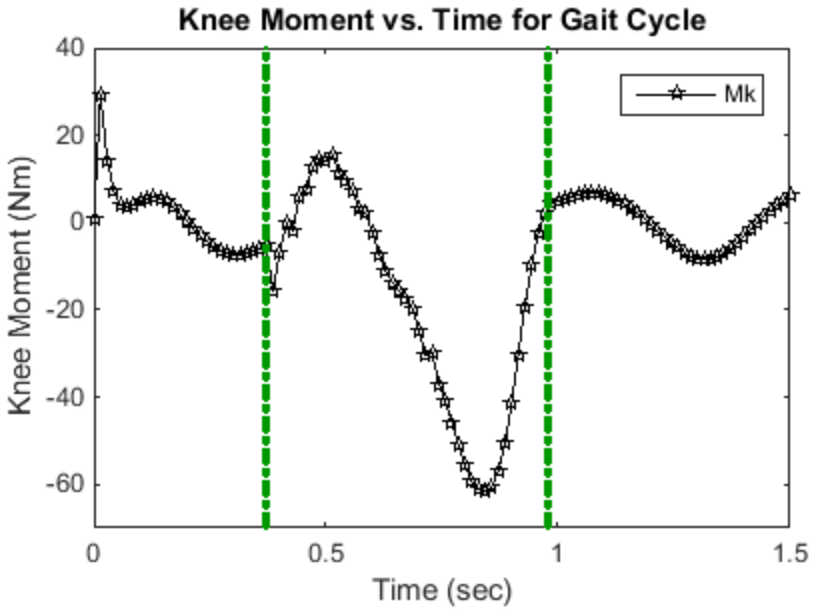

Figure 5.11 Knee moment for the gait cycle versus time, the experimental data is from (Winter, 2009) and the calculations done to obtain the knee moment (*Mk*) are from this work. In between the vertical dotted lines is the stance phase of gait, with the first dotted line representing the heel strike and the second green line representing toe off.

5.2. Squatting Numerical Simulations

Figure 5.12 shows that when comparing predictions of this work with data from (Shelburne et al., 2013) one can see that the quadriceps shows similar patterns and both reach a force of up to 4000 N and 5000 N during the ascent phase of the deep squat. However, (Shelburne et al., 2013) shows the hamstring is a stabilizing muscle which is not very active, only about 800 N throughout the ascent phase of the deep squat. The present work shows that the hamstring is a stabilizing muscle and has similar pattern throughout the ascent phase of the squat motion before the muscles reaches about 0 N when the subject is nearly standing straight up. The gastrocnemius muscle shows no activity.

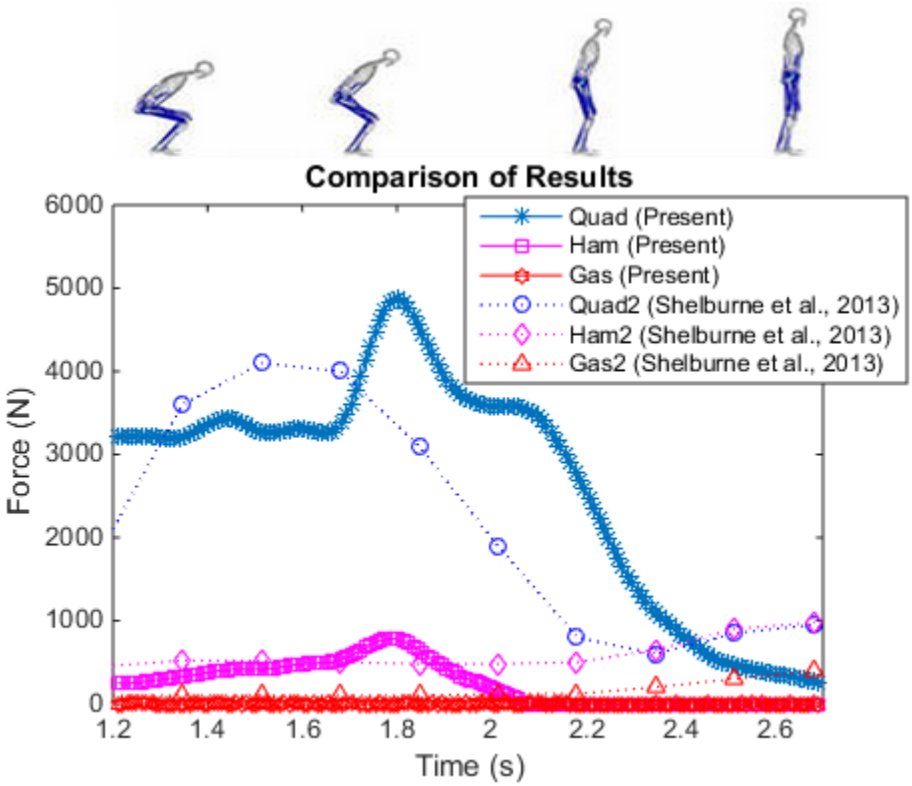

Figure 5.12 Quadriceps, hamstring and gastrocnemius forces compared with results from (Shelburne et al., 2013).

Figure 5.13 illustrates the flexion angle during a moderate squat exercise, data recorded at UTPA. The flexion angle starts at about 20˚ flexion angle, then increases to about 120˚ when the subject was at the deepest level of the moderate squat exercise (without the hamstring and the gastrocnemius touching each other), and then goes back to about 20˚.

Figure 5.14 shows the ground reaction forces (GRFs) during the moderate squat exercise. GRFs are essential for determining the other forces such as ligament, muscle and contact forces of the leg. The GRF is at about 500 N then decreases during the initial descent phase of the squat, it goes back up to about 500 N and then during the deepest part of the moderate squat the GRF increases to about 600 N, and then decreases steadily back to about 500 N during the ascending phase of the squat motion. This data has been recorded at UTPA, Biomechanics Lab.

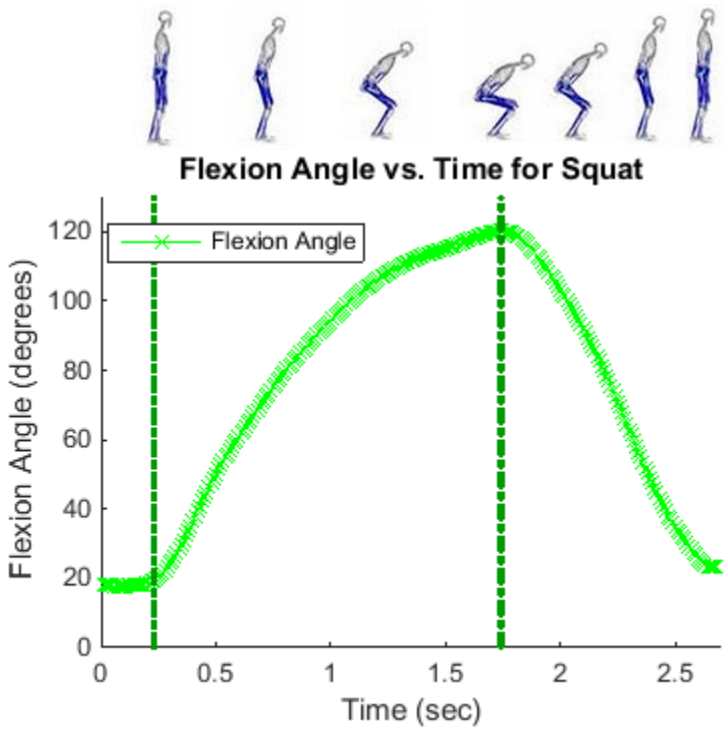

Figure 5.13 Knee flexion angle versus time for moderate squat exercise.

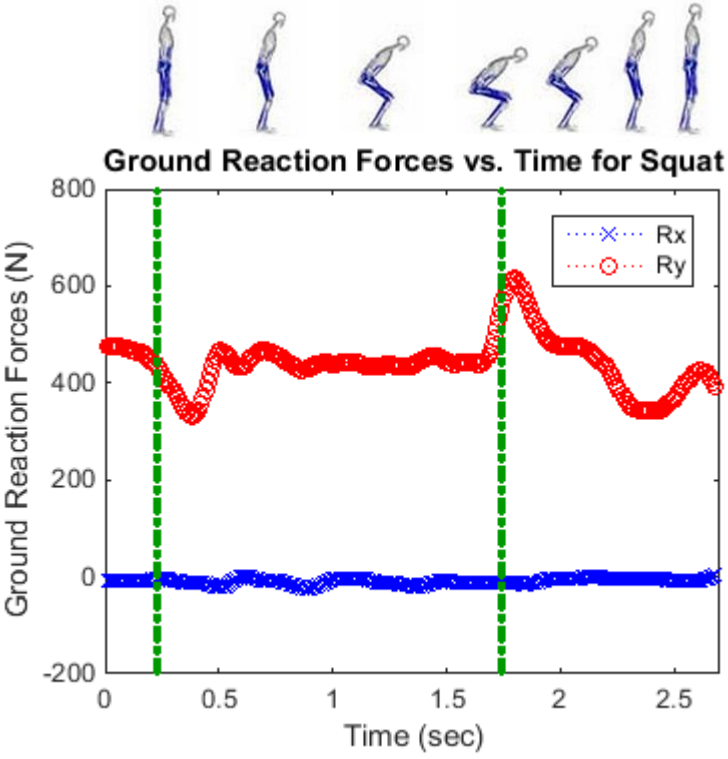

Figure 5.14 Ground reaction forces (*Rx* and *Ry*) measured during the moderate squat exercise.

Figure 5.15 shows the distance (*d*) is between the back of the tibial plateau and the femur contact point and is also an unknown. It must be assumed that these forces are greater than 0 and that "*d*" must be between 0 meters and 5 cm. The distance *d* changes throughout the moderate squat exercise. The distance *d* first starts out at about 3 cm which is the midpoint in the tibial plateau, and then throughout the squat motion this point then moves slightly anteriorly to about 4 cm in the tibial plateau, and stays in the range 4 to 5 cm for most of the exercise. This information is in good agreement with what is found in (Mukoyama, et al., 2012).

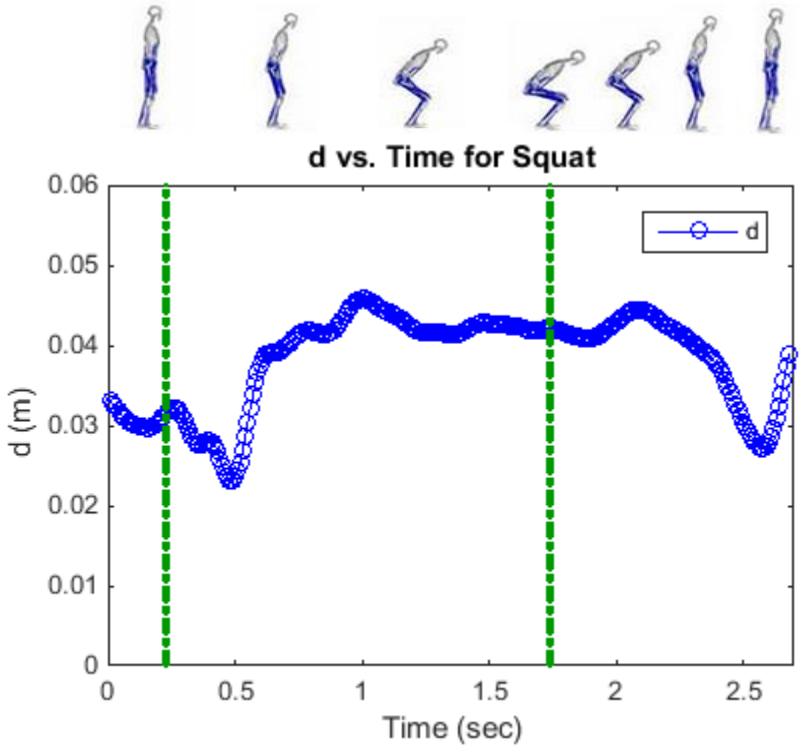

Figure 5.15 The distance (*d*) between the back of the knee plateau and the femur contact point. Assumed to be between 0 and 5 cm. 0m represents contact point at posterior position on tibial plateau and 3 cm represent contact point at center of tibial plateau.

Figure 5.16 shows the forces in the quadriceps, hamstring and gastrocnemius muscles. The quadriceps muscle shows the greatest force during the moderate squat exercise, while the

hamstring muscle, which is co-contractor muscle, shows a reduced level of activity. The quadriceps reach a force of up to about 5000 N when peak force is being applied and the hamstring force reaches to about 600 N during peak force. The gastrocnemius muscle does not show any activity during the squat exercise.

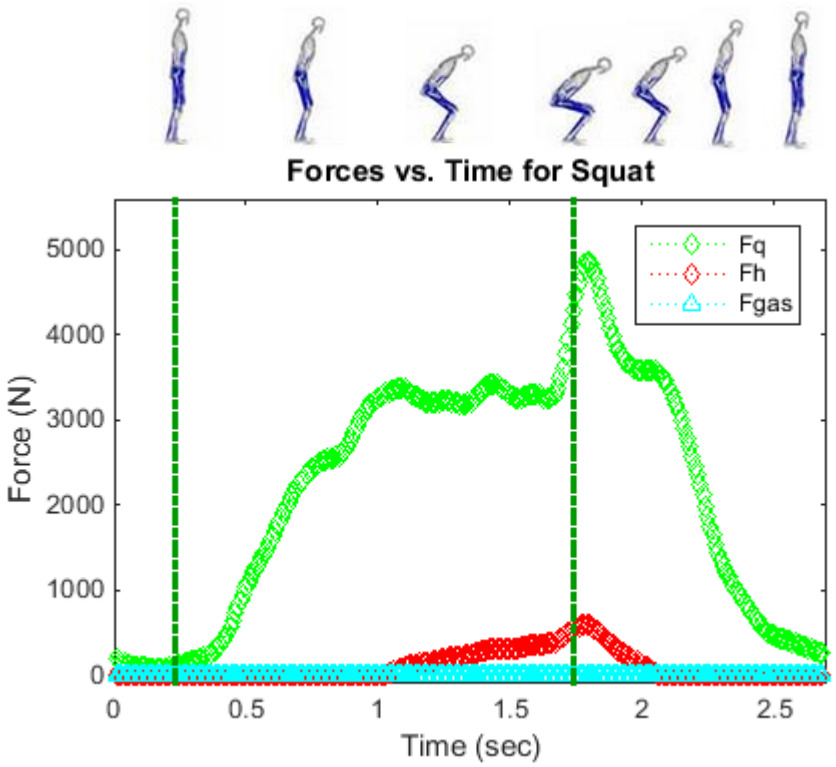

Figure 5.16 Quadriceps, hamstrings and gastrocnemius muscles during a moderate squat.

Figure 5.17 shows All the forces during the entire moderate squat exercise. All of these forces are unknowns with the exception of *Fcx*, which is assumed to be 0 N because in this work it is assume that there is no friction between tibia and femur. The greatest forces during the squat motion are shown to be *Fcy* and *Fq* which are the contact force on the tibial plateau in the y-direction and the quadriceps muscle, respectively. Both *Fcy* and *Fq* reach their peak force just after the subject reaches the point when the flexion angle is the greatest and then begins the ascent phase of the squat motion.

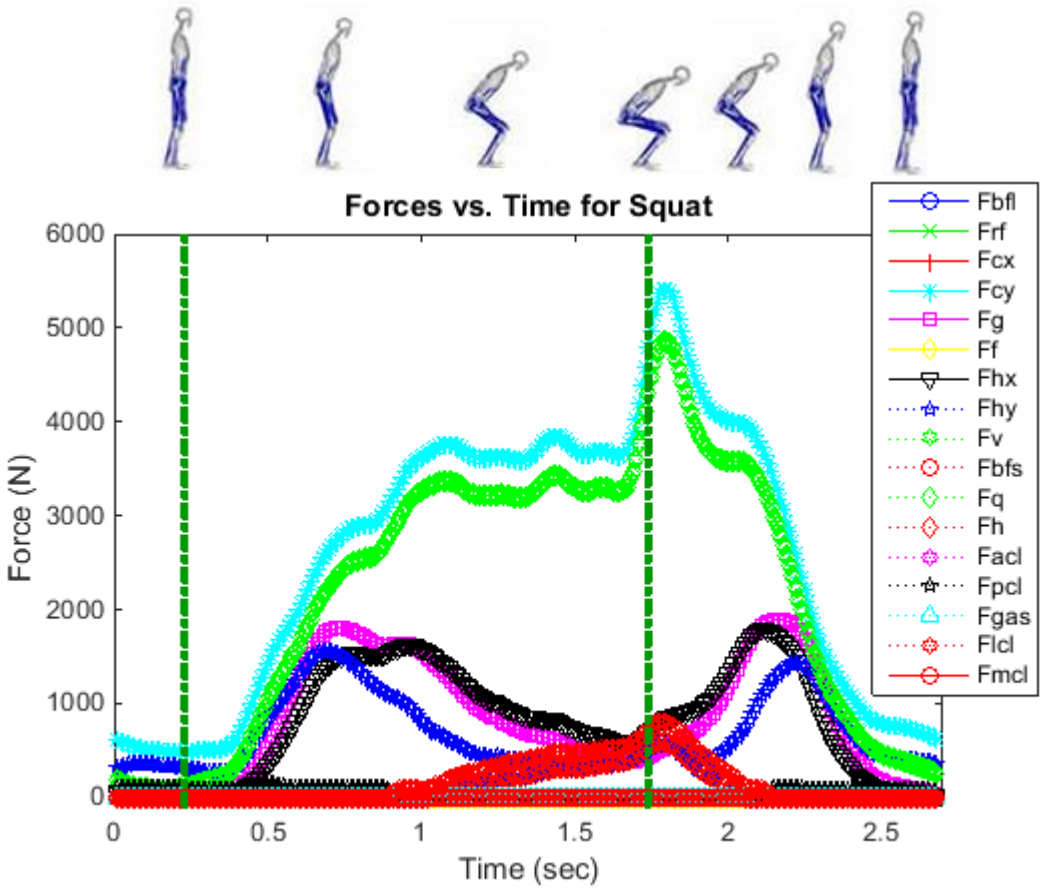

Figure 5.17 Forces versus time for squat showing the all the forces in the lower body.

Figure 5.18 shows the ligament forces during moderate squat exercise. Cruciate ligaments seem to not be active in the exercise. PCL shows little activity with a force reaching up to about 100 N during the beginning of the descent phase of the squat exercise and again during the last part of the ascent phase. MCL and the ACL do not show any activity during the squat exercise. LCL is the only ligament that shows a higher level of activity. LCL reaches a peak of about 800 N just after the largest flexion angle is reached and the subject begins the ascent phase of the squat exercise.

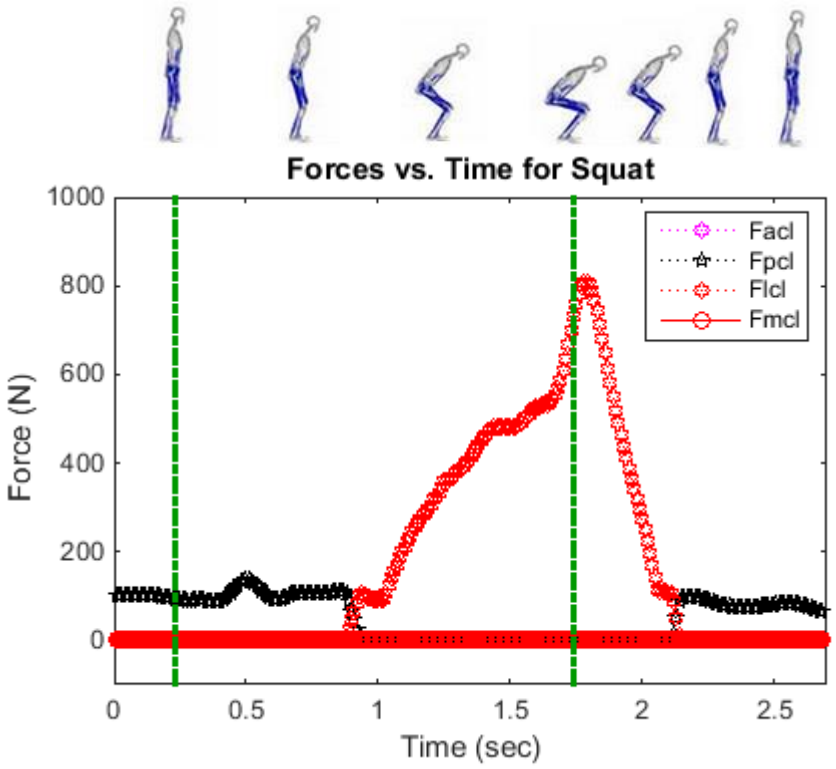

Figure 5.18 ACL, PCL, LCL and MCL ligaments forces during moderate squat exercise.

Figure 5.19 shows the joint reactions. Knee contact force *Fcy* reaches a peak around 5500 N. *Fcx* is the friction force on the tibial plateu and it is assumed to be zero, since the friction on the tibial plateau is negligible. The hip contact force along the longitudinal direction of femur *Fhy* force and the hip contact force normal to femoral axis *Fhx* show two peaks between 1600 N and 1800 N during the moderate squat exercise. One peak occurs during the descent phase of the squat motion and another peak during the ascent phase of the squat motion, one can notice that the knee contact force is the most important joint contact force in moderate squat exercise.

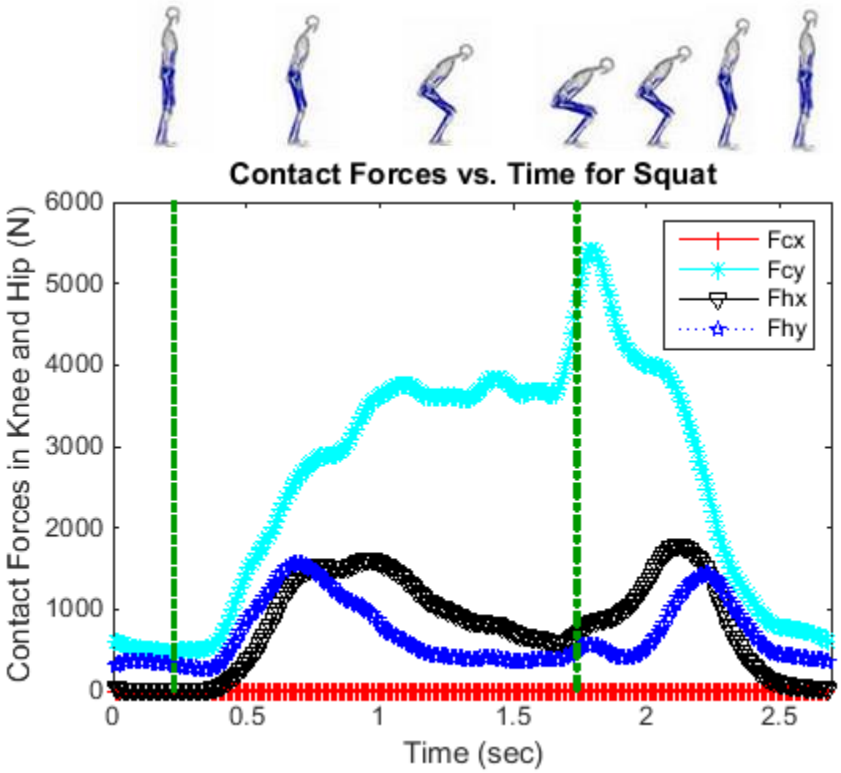

Figure 5.19 Knee (*Fcx*, *Fcy*) and hip (*Fhx*, *Fhy*) contact forces in moderate squat exercise.

Figure 5.20 shows the knee moment during the moderate squat exercise. The moment is -20 Nm when the subject is standing. As the subject descends, the moment increases to 10 Nm reaching a peak of 40 Nm when the flexion angle is at about 100˚ and the subject is just starting the ascent phase of the squat. This prediction is in good agreement with (Thambyah, 2008), which also finds the same pattern of the knee moment for squat exercise. However, he investigated deep squat motion where the flexion angle reaches up to 140˚ while in this work the flexion angle reaches up to 120˚.

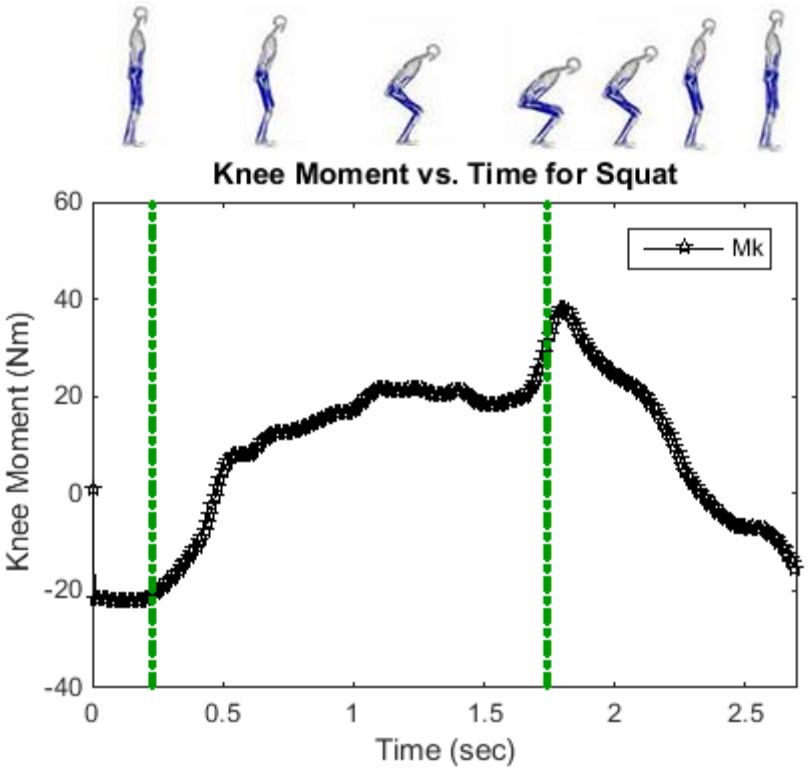

Figure 5.20 Knee moment for moderate squat exercise.

CHAPTER VI

DISCUSSION

Knee stability is vital in enhancing an athlete's performance and training, minimizing injury potential, or improving a patient's knee rehabilitation (Escamilla, 2001). Biomechanics modeling is opening new possibilities in terms of movement simulation and understanding of the interaction between the underlying structures such as bones, ligaments, tendons and muscles.

In this study it was shown that with an inverse dynamics approach model it is feasible to obtain detailed two-dimensional load distributions of knee ligaments simultaneously. The model was first used to investigate gait cycle and predict ligaments, and muscle forces. In this exercise experimental data from (Winter, 2009) was used. Each ligament plays a characteristic role in particular phases of the gait cycle. The model predictions were in agreement with data reported in the literature. There is a general consensus in the literature that the ACL and the PCL are the primary structures resisting anterior and posterior tibial loading, respectively. The ACL and PCL provide anteroposterior knee stability, while the MCL and LCL provide mediolateral knee stability. This was once more confirmed in our approach. The actual force patterns we found in the PCL during posterior loading of the tibia, however, are not compatible with the results of (Washcer et al., 1993). At a 50 N posterior tibial force, the mean PCL force was minimum at extension and increased gradually towards 58.4 N at 90˚ of flexion and the ACL force was greatest at full extension. The force patterns during the squat exercise are, however, similar to those of (Shelburne et al., 2013), who showed that the muscle forces have similar patterns.

Second, the model was used to investigate moderate squat exercise. The contact force in the knee in the y-direction (*Fcy*) shows a similar pattern as in (Smith et al., 2008) and in (Scarvell et al., 2004). However the peak force is different because they investigate deep squat exercise (calf and thigh are touching) which will reduce the forces in the knee, while in the present work the moderate squat exercise (no calf thigh touching) is investigated. (Smith et al., 2008) shows a peak of about 2400 N while this work predicts a peak of about 5500 N. Comparing ACL and PCL forces with (Toutoungi et al., 2000) in which a moderate squat is also done with the subjects doing a moderate squat with a flexion angle of 100^{o}, the ACL shows a peak of up to 27 (±35) N, the present work predicts no ACL activity during the moderate squat. PCL in (Toutoungi et al., 2000) is showed to increase during the descent phase of the squat, hit a peak of 2,500 (±800) N as the subject is at the lowest point of the squat, and then to decrease during the ascent phase. In comparison our PCL the present investigation predict a low level activity of up 100 N during the descent phase of the squat, no activity for high flexion angles of the squat, and a force of up to 100 N during the ascent phase.

The distance d locates the contact point on the tibial plateau. This work predictions show that the contact point moves anteriorly on the tibial plateau. This result is in good agreement with (Mulcahey et al., 2012) who shows that the contact point moves about 2 cm anteriorly on the Tibia as the knee flexion angle increases from 0˚ to 100˚.

6.1. Conclusions

An inverse dynamics model of the human leg has been developed. It included femur and tibia, the cruciate and collateral knee ligaments, and several leg muscles.

First, the model was used for gait cycle to investigate the internal loads in the knee joint. The results were in agreement with data reported in the literature. Second, the internal loads in

the human knee during moderate squat exercise were predicted using an inverse dynamics model of the human leg. The flexion angle is between 0 degrees to 120 degrees in this exercise. The present model predicts that during moderate squat exercise, the quadriceps experiences the highest forces of all the muscles followed by the hamstrings and then the gluteus, Fig. 5.17. The hamstrings muscle stabilizes the knee during the descent and the ascent phase of squatting. Also, the PCL is the ligament in tension during moderate squat exercise in comparison to ACL. The results showing that the PCL supports load and is active during the majority of the moderate squat exercise is useful knowledge for rehabilitation methods. For example, after ACL reconstruction, moderate squat exercises seems to be a safe exercise, which is not the case after PCL reconstruction and before healing.

6.2. Limitations

This investigation does have its limitations. First, the model is not anatomical. The femoral condyle is modeled as a circle and the tibial plateau is modeled as a straight line as shown in Fig. 6.1. Second, the model is two dimensional. Therefore the knee medial and lateral contact forces cannot be differentiated, internal-external rotation cannot be predicted. Three, the ligaments are not modeled as nonlinear springs. Therefore, although the ligament insertion points are anatomical, so anatomical ligament directions are considered, the forces in the ligaments are found through the optimization process, and not based on the elongation of the ligaments. The ligaments in the knee should be modeled as viscoelastic nonlinear springs. Four, only one set of data from one subject was used in the model.

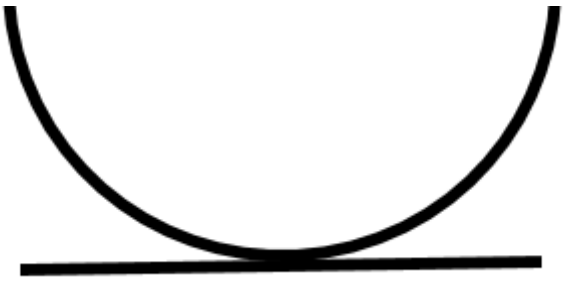

Figure 6.1 View of femoral condyle on tibial plateau.

6.3. Future Work

Further development into this research would include investigating the moderate squat exercise to include in the model patella, ligaments modeled as viscoelastic nonlinear springs, deformable contact to include articular cartilage properties, as well as several moderate squat exercise trials, and several subjects.

REFERENCES

Abdel-Rahman, E., Hefzy, M.S., 1993, "A Two-Dimensional Dynamic Anatomical Model of the Human Knee Joint," Journal of Biomechanical Engineering Vol. 115, No. 4A, pp. 357-365.

Abdel-Rahman, E.M., Hefzy, M.S., 1998, "Three-Dimensional Dynamic Behaviour of the Human Knee Joint Under Impact Loading," Medical Engineering and Physics, Vol. 20, No. 4, pp. 276-290.

Adouni, M., Shirazi-Adl, A., Shirazi, R., 2012, "Computational Biodynamics of Human Knee Joint in Gait: From Muscle Forces to Cartilage Stresses," Journal of Biomechanics **45**, pp. 2149-2156.

Akalan, N.E., Ozkan, M., Temelli, Y., 2008, "Three-Dimensional Knee Model: Constrained by Isometric Ligament Bundles and Experimentally Obtained Tibio-femoral Contacts," Journal of Biomechanics, Vol. 41, No. 4, pp. 890-896.

Amiri, S. Cooke, D., Kim, I.Y., Wyss, U., 2007, "Mechanics of the Passive Knee Joint. Part 2: Interaction between the Ligaments and the Articular Surfaces in Guiding the Joint Motion," Journal of Engineering in Medicine Vol. 221, No. 8, pp. 821-832.

Atarod, M., Rosvold, J.M., Kazemi, M., Li, L., Frank, C.B., Shrive, N.G., 2013, "Inter-insertional Distance is a Poor Correlate for Ligament Load: Analysis from in Vivo Gait Kinetics Data," Journal of Biomechanics **46**, pp. 2264-2270.

Bartel, D.L., Davy, D.T., Keaveny, T.M., "Orthopaedic Biomechanics", 2006, Pearson Prentice Hall.

Bendjaballah, M.Z., Shirazi-adl, A., Zukor, D.J., 1995, "Biomechanics of the human knee joint in compression: reconstruction, mesh generation and finite element analysis," Knee 2, pp. 69-79.

Blankevoort, L., Huiskes, R., 1991, "Ligament-Bone Interaction in a Three-Dimensional Model of the Knee," Journal of Biomechanical Engineering, 113 (1), pp. 263-269.

Blankevoort, L., Huiskes, R., 1996, "Validation of a Three-Dimensional Model of the Knee," Journal of Biomechanics, Vol. 29, No. 7, pp. 955-961.

Bei, Y, Fregly, B.J. 2004, "Multibody Dynamic Simulation of Knee Contact Mechanics," Medical Engineering & Physics, Vol. 26, No. 9, pp. 777-789.

Caruntu, D.I., Hefzy, M.S., 2004, "3-D Anatomically Based Dynamic Modeling of the Human Knee to Include Tibio-Femoral and Patello-Femoral Joints," ASME Journal of Biomechanical Engineering 126(1), pp. 44-53.

DeFrate, L.E., Sun, H. 2004, "In-vivo Tibiofemoral Contact Analysis using 3D MRI- Based Knee Models," Journal of Biomechanics Vol. 37, pp. 1499-1504.

Escamilla, R.F., 2001, "Knee Biomechanics of the Dynamic Squat Exercise," Medicine & Science in Sports & Exercise, pp. 127-141.

Gardiner, J., Weiss, J., Rosenberg, T., 2001, "Strain in the Human Medial Collateral Ligament During Valgus Lading of the Knee." Clinical Orthopaedics and Related Research 391, pp. 266-274.

Goldblatt, J.P., Richmond, J.C., 2003, "Anatomy and Biomechanics of the Knee", Journal of Operative Techniques in Sports Medicine 11(3), pp. 172-186

Halloran, J.P.; Petrella, A.J; 2005, "Explicit Finite Element Modeling of Total Knee Replacement Mechanics," Journal of Biomechanics Vol. 38, No. 2, pp. 323-331.

Hefzy, M.S., Cooke, T.D.V., 1996, "Review of Knee Models: 1996 Update," Applied Mechanics Review **49**(10), part 2, pp. 1-7.

Huss, R.A., Holstein, H., O'Connor, J.J., 2000, "A Mathematical Model of Forces in the Knee under Isometric Quadriceps Contractions," Clinical Biomechanics **15**(2), pp. 112-122.

Li, G., Lopez, O., Rubash, H., 2001, "Variability of A Three- Dimensional Finite Element Model Constructed Using Magnetic Resonance Images of a Knee for Joint Contact Stress Analysis." ASME Journal of Biomechanical Engineering, Vol. 123, No. 4, pp. 341-346.

Li, G. Vandeveldi, S.K. 2008, "Validation of a Non-Invasive Fluoroscopic Imaging Technique for the Measurement of the Dynamic Knee Joint Motion." Journal of Biomechanics, Vol. 41, No. 7, pp. 1616-1622.

Markolf, K.L., Burchfield, D.M., Shapiro, M.M., Shepard, M.F., Finerman, G.A., Slauterbech, J.L., 1995, "Combined Knee Loading States that Generate High Anterior Cruciate Ligament Forces." The Journal of Orthopaedic Research, Vol. 13, pp. 930-935.

Masouros, S.D., Bull, A.M.J., Amis, A.M.J. 2010, "Biomechanics of the Knee Joint", Orthopedics and Trauma 24(2), pp. 84-91

Mommersteeg, T.J.A; Blankevoort. L., 1996, "Characterization of the Mechanical Behavior of Human Knee Ligaments: A Numerical-Experimental Approach," Journal of Biomechanics Vol 29, No. 2, pp. 151-160.

Mukoyama, S., Yamaguchi, S., Sasho, T., Ikegawa, N., Saito, M., 2012, "Comparison of In Vivo Kinematics of the Knee between Gait and Squat," Journal of Osteoarthritis and Cartilage, Vol. 20, pp. S107-S108.

Mulcahey, M.K., Monchik, K.O., Yongpravat, C., Badger, G.J., Fadale, P.D., Hulstyn, M.J., Fleming, B.C., 2012, "Effects of Single-Bundle and Double-Bundle ACL Reconstruction on Tibiofemoral Compressive Stresses and Joint Kinematics during Simulated Squatting", The Knee, Vol. 19, pp. 469-476.

Peña, E., Calvo, B., Martinez M.A., Doblare, M., 2005, "A Three- Dimensional Finite Element Analysis of the Combined Behavior of Ligaments and Menisci in the Healthy Human Knee Joint. Journal of Biomechanics Vol. **30**, pp. 1687- 1701.

Perez-Gonzalez, A., Fenollosa-Esteve, C., Sancho-Bru, J.L., Sanchez-Marin, F.T., Vergara, M., Rodriguez-Cervantes, P.J., 2008, "A Modified Elastic Foundation Contact Model for Application in 3D Models of the Prosthetic Knee," Medical Engineering and Physics, Vol. 30, No. 3, pp. 387-398.

Ping Lim, Y., Lin, Y., Pandy, M.G., 2013, "Muscle Function during Gait is Invariant to Age When Walking Speed is Controlled," Gait & Posture **38**, pp. 253-259.

Robertson, G.A., Coleman, S.G., Keating, J.F., 2009, "Knee Stiffness Following Anterior Cruciate Ligament Reconstruction: The Incidence and Associated Factors of Knee Stiffness Following Anterior Cruciate Ligament Reconstruction," The knee, Vol. 16, No. 4, pp. 245-247.

Savio L.-Y., Woo, S.D. Abramowitch, R. Kilger, R. Liang, 2006, "Biomechanics of Knee Ligaments: Injury Healing, and Repair," Journal of Biomechanics 39, pp. 1-20.

Scarvell, J.M., Smith, P.N., Refshauge, K.M., Galloway, H.R., Woods, K.R., 2004, "Evaluation of a Method to Map Tibiofemoral Contact Points in the Normal Knee Using MRI," Journal of Orthopaedic Research, Vol. 22, pp. 788-793.

Shelburne, K.B., Fitzpatrick, C.K, Davidson, B, Laz, P.J., Christiansen, C., Stevens-Lapsley, J., Rullkoetter, P., 2013, "A Lower Extremity Model for Muscle-Driven Simulation of Activity using Explicit Finite Element Modeling," ORS Annual Meeting, Poster No: 1866

Shelburne, K.B., Pandy, M.G., 1996, "A Musculoskeletal Model of the Knee for Evaluation Ligament Forces During Isometric Contractions," Journal of Biomechanics Vol. 30, No. 2, pp. 163-176.

Shelburne, K.B., Pandy, M.G., Anderson, F.C., Torry, M.R., 2004, "Pattern of Anterior Cruciate Ligament Force in Normal Walking", Journal of Biomechanics, 37, pp. 797-805.

Smith, S.M., Cockburn, R.A., Hemmerich, A., Li, R.M., Wyss, U.P., 2008, "Tibiofemoral Joint Contact Forces and Knee Kinematics During Squatting," Gait and Posture, Vol. 27, pp. 376-386.

Sugita, T., Amis, A.A., 2001, "Anatomic and Biomechanical Study of the Lateral Collateral Ligament and Popliteofibular Ligaments," The American journal of sports medicine, Vol. 29, No. 4, pp. 466-472.

Thambyah, A., 2008. "How Critical are the Tibiofemoral Joint Reaction Forces During Frequent Squatting in Asian Populations?" The Knee, Vol. 15, pp. 286-294.

Toutoungi, D.E., Lu, T.W., Leardini, A., Catani, F., O'Connor, J.J., 2000, "Cruciate Ligament Forces in the Human Knee During Rehabilitation", Journal of Clinical Biomechanics, Vol. 15, pp. 176-187.

Vaziri, A; Nayeb-Hashemi, H; 2008, "Influence of Meniscectomy and Meniscus Replacement on the Stress Distribution in Human Knee Joint", Biomechanical Engineering Society Vol. 36 No. 8. pp. 1335-1444.

Washcer, D.C., Markolf, K.L., Shapiro, M.S., Finerman, G.A., 1993, "Direct in Vitro Measurement of Forces in the Cruciate Ligaments: I. The Effect of Multi-Plane Loading in the Intact Knee," Journal of Bone and Joint Surgery, Vol. 75A, No. 3, pp. 377-386.

Weinstein, A.M., Rome, B., Reichmann, W.M., Collins, J.E., Burbine, S.A., Thornhill, T.S., Wright, J.J., Katz, J.N., Losina, E., 2012, "How many Americans are Currently Living with Total Knee Replacement?" American Academy of Orthopaedic Surgeons, Session 54, Presentation Number 797

White, S.C., Winter, D.A., 1993, "Predicting Muscle Forces in Gait from EMG Signals and Musculotendon Kinematics," Journal of Electromyography and Kinesiology, Vol. 2, No. 4, pp. 217-231.

Winiarski, S., Kucharska, A.R., 2009, "Estimated Ground Reaction Force in Normal and Pathological Gait", Acta of Bioengineering and Biomechanics, Vol. 11, No. 1, pp. 53-60.

Winter, D.A., "Biomechanics and Motor Control of Human Movement," 4th Edition, 2009, Wiley.

BIOGRAPHICAL SKETCH

Ricardo Gomez Jr. was born in McAllen, TX on March 14, 1987. He attended James Nikki Rowe High School in McAllen, TX, graduating in 2005. He attended the University of Texas – Pan American, Edinburg, TX, first earning a Bachelors of Science degree in Mechanical Engineering in 2012. Most recently he has attended the University of Texas – Pan American in Edinburg, TX, receiving a Masters of Science in Mechanical Engineering during the Summer of 2015. As a graduate student, from August 2013 to May 2014, he worked as a mechanical engineer intern at Texas Manufacturing Assistance Center with the primary role of optimizing energy usage at a water treatment plant. He currently resides at 5808 N 23rd St., McAllen, TX 78504.